Geochimica Et Cosmochimica Acta
September 2022, Volume 333 Pages 136-152
https://doi.org/10.1016/j.gca.2022.06.038
https://archimer.ifremer.fr/doc/00785/89731/

Light Zn and Cu isotope compositions recorded in ferromanganese crusts during the Cenozoic as evidence for hydrothermal inputs in South Pacific deep seawater

Gueguen Bleuenn [1, 2, *], Rouxel Olivier [3], Fouquet Yves [3]

[1] Univ Brest, CNRS, UMS 3113, IUEM, Place Nicolas Copernic, 29280 Plouzane, France
[2] Univ Brest, CNRS, UMR 6538, Geo-Ocean UMR 6538, IUEM, Place Nicolas Copernic, 29280 Plouzane, France
[3] IFREMER, Centre de Brest, Geo-Ocean UMR 6538, F-29280 Plouzane, France

* Corresponding author : Bleuenn Gueguen, email address : bleuenn.gueguen@univ-brest.fr

Abstract :

This study presents a high-resolution record of Cu and Zn isotopes in four Fe-Mn crusts from the North and South Pacific oceans. North Pacific crusts were collected on the Apuupuu seamount south of the Hawaiian archipelago and South Pacific crusts were recovered near Rurutu Island in the Tahiti archipelago. Major and trace element compositions suggest that Cu and Zn in these crusts is of hydrogenous origin, i.e., precipitated from seawater, and they may therefore mirror deep seawater metal isotope. We show that Cu and Zn display different isotopic patterns between the North and the South Pacific Oceans but show similar temporal evolution within each geographical area. Copper and Zn isotope composition of both North Pacific crusts vary between 0.57 ‰ to 0.73 ‰ for δ65/63CuNIST976 and 0.97 ‰ to 1.25 ‰ for δ66/64ZnJMC-Lyon. In contrast, South Pacific crusts show resolvable temporal variations, with Cu and Zn isotopic ratios increasing sharply over the last ~ 6 Ma from 0.16 ‰ to 0.51 ‰ and 0.67 ‰ to 1.09 ‰ respectively. Notably, we observed a positive correlation between δ65/63CuNIST976 and δ66/64ZnJMC-Lyon values in Fe-Mn crusts from the South Pacific. The correlation suggests mixing between two components in Fe-Mn crusts, a hydrothermal component with δ65/63CuNIST976 ~ 0.2 ‰ and δ66/64ZnJMC-Lyon ~ 0.7 ‰, and a Pacific deep seawater component with δ65/63CuNIST976 ~ 0.7 ‰ and δ66/64ZnJMC-Lyon ~ 1.2 ‰. These values are fractionated from modern dissolved Cu and Zn by a factor of −0.3 ‰ and 0.5 ‰ respectively. We suggest that the deep Southern Pacific Ocean received sustained hydrothermal input during the last 6 Ma, which was recorded in the Cu and Zn isotope composition of Fe-Mn crusts precipitated thousands of kilometers away. Our study highlights that hydrothermal venting may be a significant source of Cu and Zn in the deep oceans despite their extensive precipitation within hydrothermal vent fields. We show that this source could be persistent through time, and thus, it could have a significant impact on the biogeochemical cycling of Cu and Zn in seawater which would ultimately be recorded by Fe-Mn crusts.

Keywords : Ferromanganese crusts, Copper isotopes, Zinc isotopes, hydrothermal inputs

1. Introduction

Our understanding of metal biogeochemical cycles in the oceans has increased significantly since the development of methods for measuring low trace metal concentrations in seawater (e.g., Bruland et al., 1994; Sohrin et al., 1998; Sohrin et al., 2008; Sohrin and Bruland, 2011; Biller and Bruland, 2012; Minami et al., 2015; Yang et al., 2020). Surface bioproductivity has long been recognized as an important parameter influencing distribution of transition metals in seawater because many of those trace elements are essential, and in some cases bio-limiting, for primary productivity (e.g., Fe, Zn, Cd, Ni; Morel and Price, 2003). However, our knowledge of the deep ocean biogeochemical cycling of metals is relatively incomplete, in particular with respect to benthic sources and oceanic water masses dynamics. For instance, the importance of hydrothermal inputs for the oceanic Mn, Fe, Zn and Cu budgets has been demonstrated to be important in the South Pacific, notably because of hydrothermal vents along the fast spreading South East Pacific Rise (EPR) that contribute to large hydrothermal fluxes in seawater (Boström et al., 1969; Lupton and Craig, 1981; Baker and Massoth, 1986; Baker et al., 1995; Urabe et al., 1995; Lupton, 1998; Tagliabue et al., 2010; Hannington, 2013; Fitzsimmons et al., 2014; Resing et al., 2015; Roshan et al., 2016; John et al., 2018). Variations of these fluxes through time could potentially have an influence on global metal biogeochemical cycles.

Among these trace metals, particular attention is now given to Cu and Zn as new biogeochemical tools (e.g., see review by Moynier et al., 2017). These elements are mostly supplied to oceans via riverine input from the continents, whereas the most important sink is associated with the precipitation of Fe-Mn-oxides at the seafloor (Little et al., 2014; Little et

al., 2016; Vance et al., 2016). Dissolved Zn exhibits a nutrient-type profile in seawater as a result of biological uptake in surface waters and recycling of settling organic matter in deep waters (Bruland, 1980; Bruland, 1983; Morel and Price, 2003). The importance of Zn for biological activity is also shown by the close relationships between Zn cycling and phosphate in the Southern Ocean for example (Sieber et al., 2020), and silicate cycling (e.g., Bruland, 1980; Samanta et al., 2017; Vance et al., 2017; Weber et al., 2018; Lemaitre et al., 2020). By contrast, dissolved Cu behaves as a "hybrid-type" element, i.e. a particle-reactive element that can be partially scavenged and partially used in biological activity (Bruland et al., 2014), and its concentration in the water column increases with depth (Boyle et al., 1977; Bruland, 1980). In addition, most dissolved Zn and Cu in the marine environment are complexed to strong organic ligands (e.g., Coale and Bruland, 1988; Bruland, 1989; Moffett and Dupont, 2007; Horner et al., 2021b).

Subsequent to the development of efficient methods for measuring metal concentration in seawater, many studies have reported seawater Cu and Zn isotope compositions of the dissolved phase (e.g., Bermin et al., 2006; Vance et al., 2008; Conway et al., 2013; Conway and John, 2014; Zhao et al., 2014; Little et al., 2018; Baconnais et al., 2019; Vance et al., 2019; Lemaitre et al., 2020; Liao et al., 2020). Biological activity fractionates Zn isotopes and may impart heavier isotope signatures to surface waters in the water column (Zhu et al., 2002; John et al., 2007; Andersen et al., 2011; Samanta et al., 2017; Köbberich and Vance, 2019). Some studies therefore suggest that Zn isotopic signatures might be used to trace primary productivity in the sedimentary archive, e.g., in carbonates (Pichat et al., 2003; Kunzmann et al., 2013). However, recent studies of Zn isotopes in modern seawater have revealed a more complex picture. For example, in the Southern Ocean, uptake of Zn by diatoms does not necessarily produce an isotopically heavy surface seawater (Zhao et al., 2014), while in the North Pacific Ocean light Zn isotope compositions in some surface waters may be attributed

to intracellular regeneration of light Zn isotopes (Conway and John, 2014; Zhao et al., 2014). Scavenging and adsorption of Zn onto organic matter may also have an important role in the cycling of Zn isotopes in surface waters (John and Conway, 2014; John et al., 2018; Weber et al., 2018) in addition to aerosol and anthropogenic sources (Conway and John, 2014; Lemaitre et al., 2020; Liao et al., 2020). No clear and systematic effects have been observed due to biological uptake in the water column for Cu isotopes (e.g., Vance et al., 2008; Takano et al., 2014; Little et al., 2018; Baconnais et al., 2019; Yang et al., 2020), but light Cu isotope compositions in surface waters have been attributed to local sources such as aeolian particles and particulates from rivers and sediments (Takano et al., 2014; Little et al., 2018).

In the deep ocean, despite relatively homogenous isotopic composition for Zn with an average value of 0.5 ±0.1 ‰ (e.g.; Boyle et al., 2012; Conway et al., 2013; Conway and John, 2014, 2015; Takano et al., 2017; John et al., 2018; Vance et al., 2019), and Cu with an average value of ~0.7 ‰ (e.g.; Boyle et al., 2012; Takano et al., 2013, 2014; Takano et al., 2017; Little et al., 2018; Baconnais et al., 2019); these studies show that deep sources of Zn and Cu may have an impact on isotopic signatures. For example, the influence of hydrothermal inputs on Zn in seawater has been demonstrated by a few studies in the North Atlantic Ocean (Conway and John, 2014; Lemaitre et al., 2020) and in the South Pacific Ocean (Roshan et al., 2016; John et al., 2018). They show that isotopically light Zn is released in the deep ocean and could be transported over a few thousands of kilometers, and this input flux could, in fact, be a predominant source of Zn.

Experimental results of Syverson et al. (2021) showed that chalcopyrite precipitates at equilibrium conditions at 350°C and is isotopically fractionated from dissolved Cu by -0.22 ±0.16 ‰. This suggests that the Cu remaining in the hydrothermal fluids released in seawater is enriched in heavy isotopes. Furthermore, studies show that Cu could be transported far from the hydrothermal source producing significant Cu enrichment in the sediment

(Hannington, 2013). This shows that deep local sources such as hydrothermal venting could contribute significantly to the biogeochemical cycling of Cu and Zn through time. However, how Cu can be transported from the hydrothermal vent is not clear yet. Models indicate that Cu can be transported through complexation in organic ligands (Sander and Koschinsky, 2011), but this has not been observed on the field yet. Observations indicate that most of the dissolved Cu is precipitated near the vent (Roshan and Wu, 2015), and GEOTRACES data only indicate an increase in particulate Cu (GEOTRACES Intermediate Data Product Group, 2021).

A promising target for investigating metal biogeochemical cycling and isotopic compositions of deep waters over longer time scale is the hydrogenetic ferromanganese (Fe-Mn) crusts archive. These metalliferous deposits are composed of a mineralogical assemblage of Mn- and Fe-oxides, which are highly enriched in Ni, Co, Cu, Zn, Mo, Te, Pt, Tl relative to the average continental crust (e.g.; Li and Schoonmaker, 2003; Hein et al., 2010; Hein et al., 2013). The well accepted model for explaining metal enrichment is that metals are exclusively derived from seawater through precipitation of hydrogenous Fe- and Mn-oxyhydroxides. The process of Fe-Mn crusts formation is promoted by the presence of an Oxygen Minimum Zone (OMZ) in the water column, which allows accumulation of soluble reduced Mn^{2+} due to low oxygen concentrations (Koschinsky and Halbach, 1995). The term Oxygen Minimum Zone (OMZ) has been used to refer to regions, typically along upwelling continental margins, with very depleted oxygen concentrations of < 20 μM (Paulmier and Ruiz-Pino, 2009). However, low oxygen concentrations, of about 50-100 μM, are found throughout the oceans at 1000 to 1500 m water depths, and have also classically been termed “OMZs”. Here, we adopt the term OMZ to refer to the latter, i.e., low oxygen regions throughout intermediate depths of the world oceans. Upon recycling of the dissolved Mn out of the OMZ, Mn is re-oxidized and form colloids to scavenge dissolved trace metals. Colloids provide nucleation sites for the

formation of Mn-oxides at the surface of rocks of the seafloor, and then ferromanganese crusts grow through incorporation of dissolved metals. They are generally precipitated at very slow growth rates between 1 and 6 mm/Ma on the flank of seamounts (but some are formed on a sedimentary substrate), which serves as a substrate for Fe-Mn encrustations at depths between 1000 and 3000 meters. Ferromanganese crusts grow in low sedimentation rates areas in order to prevent transition metals dilution by terrigenous and calcareous particles (Halbach et al., 1983; Hein et al., 1988; Hein et al., 1992; Koschinsky and Halbach, 1995; Koschinsky et al., 1997). To date, Fe-Mn crusts deposits have been intensively investigated for their radiogenic isotope composition (Pb, Nd, Hf) for tracing the evolution of oceanic circulation and its relation to climate variations and continental fluxes of material to oceans (see for example the review by Frank, 2002). During the last decade, studies focusing on transition metal isotope systematics records in Fe-Mn crusts have blossomed (e.g., see reviews by; Fu, 2020; Horner et al., 2021a), including Fe (Zhu et al., 2000; Levasseur et al., 2004; Chu et al., 2006; Horner et al., 2015), Tl (Rehkämper et al., 2002; Rehkämper et al., 2004), Cd (Schmitt et al., 2009; Horner et al., 2010), Mo (Siebert et al., 2003), Ni (Gall et al., 2013; Gueguen et al., 2016) and Cu and Zn (Maréchal et al., 2000; Albarède, 2004; Little et al., 2014). Published data on Cu and Zn isotopes in oceanic metalliferous deposits display a significant range of values, i.e., $\delta^{65/63}Cu_{NIST976}$ = 0.31± 0.23 ‰ and $\delta^{66/64}Zn_{JMC\text{-}Lyon}$ = 0.90 ± 0.28 ‰ in Mn-nodules (Maréchal et al., 2000; Albarède, 2004); and $\delta^{65/63}Cu_{NIST976}$ = 0.44± 0.23 ‰ and $\delta^{66/64}Zn_{JMC\text{-}Lyon}$ = 1.04 ± 0.21 ‰ in Fe-Mn crusts (Little et al., 2014), although the causes of such isotopic variations remain largely unresolved. Therefore, in Fe-Mn deposits Cu isotopes are on average 0.3 ‰ lighter and Zn isotopes are 0.5 ‰ heavier compared to seawater. In addition to source variations, adsorption mechanisms may be also important (Little et al., 2014b; Bryan et al., 2015; Sherman and Little, 2020), complicating paleo-oceanographic reconstructions.

Here, we investigated spatial and temporal variations of Cu and Zn isotope compositions in four hydrogenetic Fe-Mn crusts from the Pacific Ocean in order to understand the possible factors responsible for Cu and Zn isotope variations in the deep ocean through time.

2. Materials and methods

2.1. Sample description

2.1.1. Microsampling of Fe-Mn crusts from the North and South Pacific Ocean

Four Fe-Mn crusts were selected for generating high-resolution depth profiles through microsampling of Fe-Mn crusts layers. Detailed description of the samples has already been published in Gueguen et al. (2016). Briefly, the sample set comprises two Fe-Mn crusts collected in the North Pacific on Apuupuu seamount ~50 km south of Hawaii during FeMO 2009 cruise on the R/V Kilo Moana (University of Hawaii) in October 2009, and two Fe-Mn crusts collected in the South Pacific (Tahiti, Austral archipelago of French Polynesia) near Rurutu Island by dredges during ZEPOLYF 2 cruise on the R/V L'Atalante (Ifremer-Genavir) in July-August 1999 (Table 1). The North Pacifc Fe-Mn crusts (J2-480 and J2-480-R14) were collected at 2079 m depth while the South Pacific Fe-Mn crusts were collected at shallower depths at 1826 m and 1530 m (ZEP2-DR-05-04 and ZEP2-DR-06-03 respectively).

Each crust was split and a representative cross section was taken off (including whenever it was possible the top surface) and embedded into epoxy resin and polished. Growth layers of Fe-Mn crusts were subsampled at mm-scale using a microdrilling device (Micromill®). Lines perpendicular to the direction of growth were drilled to obtain sufficient crust powder for geochemical analyses. The total amount of powder collected in each line was

197 generally between ~30 and 50 mg. Details on sample processing can be found in Gueguen et
198 al. (2016) as well as dating of the crusts which was made using cosmogenic ^{10}Be isotope
199 measurements (Segl et al., 1984; Bourles et al., 1989). Fe-Mn crust ZEP2-DR05-04 could not
200 be dated with ^{10}Be because the base of the crust has been affected by post-deposition
201 alteration which has reset the chronometer. ZEP2-DR05-04 was therefore dated using Co
202 accumulation rates in the Fe-Mn crust (see explanations in Gueguen et al., 2016).
203
204 *2.1.2. Bulk ferromanganese crusts*
205
206 Additional bulk Fe-Mn crusts samples from various locations including Pacific and
207 Atlantic Oceans completed the dataset of this study. Description of samples is reported in
208 Gueguen et al. (2021). Fe-Mn crusts from the Atlantic Ocean were sampled at different
209 locations, along the Ascension Fracture Zone (FZ), VEMA FZ, Gloria FZ and the Azores
210 Triple Junction (TJ). Even if these samples do not strictly reflect the bulk crusts because they
211 consist of subsamples collected at different depths within the crust and this depth is different
212 according to samples, the resolution of sampling and the size of sample are large enough to be
213 considered as a bulk sample. As a consequence, no attempts were made to give age range for
214 these samples. Two additional Fe-Mn crusts collected in the North Pacific from Apuupuu
215 seamounts were also selected as bulk Fe-Mn crust samples (recovered during the same
216 cruise).
217
218 *2.3. Cu and Zn isotopes analyses*
219
220 Copper and Zinc isotope compositions were measured at Pôle-Spectrométrie-Océan
221 (PSO, Ifremer, Brest, France) by MC-ICP-MS (Neptune, Thermofisher Scientific). Copper

and Zinc isotope ratios were corrected with internal isotopic standards of Zn NIST SRM 3168a and Cu NIST SRM 976 respectively, doped in samples prior to analysis coupled to a standard-sample-bracketing procedure (Marechal et al., 1999; Albarède, 2004).

The fractionation factor calculated for the doped element for which the isotope composition is known is applied to the isotopic ratios of the measured element assuming that isotopes of both the doped element and the element to be measured follow a similar exponential mass fractionation law (Marechal et al., 1999; Albarède, 2004). Prior to isotope analyses on the mass spectrometer, Cu and Zn were separated with ion-exchange chromatography columns using AG-MP1 resin. Two milliliters of resin were loaded in polypropylene columns. A split from the sample archive solutions was taken off and evaporated to dryness on hot Teflon plates and redissolved in 1.2 mol/L HCl and then loaded on the resin. Both Cu and Zn were purified twice through the columns. Samples were prepared to target 100 ng of Cu and Zn for MC-ICP-MS measurements. Procedural blanks measured were <0.3 ng for Cu and <3 ng for Zn.

Isotopic compositions are expressed as $\delta^{65/63}Cu_{NIST976}$ and $\delta^{66/64}Zn_{JMC\text{-}Lyon}$ (‰) using respectively the following equations (1) and (2) :

$$\delta^{65/63}Cu_{NIST976} = [(^{65}Cu/^{63}Cu_{sample})/(^{65}Cu/^{63}Cu_{NIST976}) - 1] \times 1000 \quad (1)$$

$$\delta^{66/64}Zn_{JMC\text{-}Lyon} = [(^{66}Zn/^{64}Zn_{sample})/(^{66}Zn/^{64}Zn_{JMC\text{-}Lyon}) - 1] \times 1000 \quad (2)$$

Precisions on the Cu and Zn isotope delta values are reported as a two-standard deviation (2sd) calculated on replicate measurements of the isotopic standards Cu NIST SRM 976 and Zn NIST SRM 3168a respectively (Table 1), following a standard-sample bracketing method. Zinc isotope values are generally reported relatively to the JMC Lyon Zn standard

and Archer et al. (2017) proposed to keep this notation to allow for a direct comparison with all published data. Based on an inter-calibration exercise (Archer et al., 2017), JMC Lyon Zn isotopic standard is fractionated relative to Zn AA-ETH standard by 0.28‰ and to Zn NIST SRM 3168a standard by 0.94 ‰.

We also performed replicate analyses of Geological Reference Materials (GRMs) Nod-A-1 and Nod-P-1 which yield, respectively, average values of 0.29 ±0.09 ‰ (2sd, n=4) and 0.34 ±0.05 ‰ (2sd, n=5) for $\delta^{65/63}Cu_{NIST976}$ and 0.95 ±0.07 ‰ (2sd, n=4) and 0.80 ±0.12 ‰ (2sd, n=5) for $\delta^{66/64}Zn_{JMC\text{-}Lyon}$ (Table 1). The values are consistent with published data (Chapman et al., 2006; Bigalke et al., 2010; Little et al., 2017). Errors reported for the GRMs in Table 1 correspond to the two-standard deviation of the replicate analyses of each GRM. These replicates include different digested aliquots and duplicates from the chromatography column separation procedure.

3. Results

Description of the trace element data and determination of the age the Fe-Mn crusts are reported in Gueguen et al. (2016). The four Fe-Mn crusts are typical hydrogenetic Fe-Mn crusts and fall in the hydrogenetic field of the ternary diagram of Bonatti et al. (1972). Copper and Zn concentrations covary with Mn concentrations suggesting that Cu and Zn are hosted by the Mn-phase. Therefore, we chose to present in this study elemental ratios with elements normalized to Mn in order to avoid potential dilution by other mineral phases present in the crusts. Mn/Fe ratios (Table 1 and supplementary information) in North Pacific Fe-Mn crusts show a significant increase through time between ~10 Ma and ~8 Ma from 0.68 to 2.22 in J2-480 and from 1.25 to 1.79 in J2-480-R14. Fe-Mn crusts from South Pacific also exhibit an increase in Mn/Fe ratios from ~4 Ma to the top of the crust from 0.98 to 1.45 in ZEP2-DR06-

03 and from 0.99 to 1.91 in ZEP2-DR05-04. Zn/Mn and Cu/Mn ratios are similar in both South Pacific Fe-Mn crusts, and display a continuous decrease from the "bottom" region (i.e., older portion of the crust) to the "top" region (i.e., younger portion of the crust). In contrast, North Pacific Fe-Mn crusts display opposite trends in Zn/Mn ratios although both crusts show similar features with a sharp increase ca. 6 Ma (Figure 1). Fe-Mn crusts from the North Pacific on the one hand, and South Pacific on the other hand show similar decrease in Cu/Mn ratios. The highest Cu/Mn ratios are observed for the oldest sub-samples of J2-480 (>10Ma), a time period not covered by South Pacific Fe-Mn crusts (Figure 1).

The Cu and Zn isotope compositions in both North Pacific Fe-Mn crusts show a relatively restricted range of variations with values of 0.57 ±0.06 ‰ to 0.67 ±0.06 ‰ for $\delta^{65/63}Cu_{NIST976}$ and 0.97 ±0.04 ‰ to 1.25 ±0.04 ‰ for $\delta^{66/64}Zn_{JMC\text{-}Lyon}$ in J2-480, and from 0.56 ±0.06 ‰ to 0.72 ±0.06 ‰ for $\delta^{65/63}Cu_{NIST976}$ and 1.15 ±0.04 ‰ to 1.25 ±0.04 ‰ for $\delta^{66/64}Zn_{JMC\text{-}Lyon}$ in J2-480-R14 (Table 1 and Figure 2). In contrast to North Pacific Fe-Mn crusts, South Pacific Fe-Mn crusts show significant isotopic variability over the last 10 Ma. First, there is a concomitant increase in $\delta^{65/63}Cu_{NIST976}$ and $\delta^{66/64}Zn_{JMC\text{-}Lyon}$ at about 6 Ma to 4 Ma, from 0.16 ±0.03 ‰ to 0.51 ±0.03 ‰ for $\delta^{65/63}Cu_{NIST976}$ and from 0.67 ‰ ±0.03 to 1.09 ±0.03 ‰ for $\delta^{66/64}Zn_{JMC\text{-}Lyon}$ values (Table 1 and Figure 2). This translates into a strong positive correlation between $\delta^{65/63}Cu_{NIST976}$ and $\delta^{66/64}Zn_{JMC\text{-}Lyon}$ values (Figure 3) with a correlation coefficient R^2=0.90 (Figure 3). Second, the Cu and Zn isotope compositions of the South Pacific Fe-Mn crusts (which essentially control the positive correlation in Figure 3) become heavier with time. Figure 3 also includes the isotopic compositions of bulk Fe-Mn crusts. $\delta^{65/63}Cu_{NIST976}$ values in bulk Fe-Mn crusts are comprised between 0.15 ‰ and 0.54 ‰ with an average value of 0.28 ±0.13 ‰ (2sd, n=20) while $\delta^{66/64}Zn_{JMC\text{-}Lyon}$ values range from 0.58 ‰ to 1.03 ‰ around an average value of 0.80 ±0.15 ‰ (2sd, n=20) which encompasses the range measured in the four Fe-Mn crusts time-series of this study.

297 Figure 4 shows that light $\delta^{65/63}Cu_{NIST976}$ and $\delta^{66/64}Zn_{JMC\text{-}Lyon}$ values in South Pacific Fe-
298 Mn crusts (ZEP2-DR05-04 and ZEP2-DR06-03) are correlated with higher Cu/Zn ratios
299 whereas such correlation does not exist in North Pacific Fe-Mn crusts (J2-480 and J2-480-
300 R14) displaying constant Cu and Zn isotope values for variable Cu/Zn ratios. The range of
301 Cu/Zn ratios (0.75 to 2.66) is similar in both South Pacific and North Pacific Fe-Mn crusts
302 and the four crusts show decreasing Cu/Zn ratios from older to younger crust (Table 1). In a
303 previous paper, Gueguen et al. (2016), it was shown that the last four samples of ZEP2-DR05-
304 04 have been subjected to post-deposition alteration. Although the Cu and Zn isotope patterns
305 are not changed by these alteration processes (see Table 1), we have chosen not to represent
306 these four data-points in the figures of the manuscript.
307
308 **4. Discussion**
309
310 *4.1 Significance of Cu and Zn isotope co-variations in ferromanganese crusts*
311
312 Ferromanganese crusts are precipitated from trace metals dissolved in seawater. Thus,
313 isotopic variations recorded in the crusts are the result of either in-situ fractionation during
314 precipitation of the crust (e.g., adsorption, growth rates) or late alteration of the crust, or to
315 variable seawater isotopic composition through time (e.g., oceanic circulation, sources of
316 trace metals to seawater). Since a positive correlation between Cu and Zn isotopes is observed
317 in the two South Pacific Fe-Mn crusts, it is likely that the causes of both Cu and Zn isotope
318 variations are intimately coupled. The correlation may result either from, (1) isotopic
319 fractionation during growth (e.g., sorption) or post-depositional alteration of the crusts, with
320 preferential fractionation of the light (or heavy) isotopes of both Cu and Zn, or, (2) mixing of

two sources with distinct Cu and Zn isotope compositions. The relative importance of each process is discussed below.

The primary Zn and Cu hosting Mn oxide phases in hydrogenetic Fe-Mn crusts are poorly crystallized phyllomanganate phases, typically vernadite (δ-MnO_2, also often called birnessite). Experimental results of Zn isotope fractionation during sorption to Mn-oxides birnessite indicate that isotopically heavy Zn (up to ~3 ‰) is sorbed to the mineral surface (Bryan et al., 2015), consistent with the fact that Zn isotopes in ferromanganese crusts (Little et al., 2014) are on average 0.5 ‰ heavier than seawater (Boyle et al., 2012; Conway and John, 2014; Zhao et al., 2014; Conway and John, 2015; Lemaitre et al., 2020). Adsorption of Cu onto synthetic birnessite results in preferential fractionation of the light isotopes on the solid phase by a factor of -0.45 ±0.18 ‰ (Ijichi et al., 2018). On the other hand, Sherman and Little (2020) found that dissolved Cu isotope composition should be 0.94 ‰ (at 5°C) heavier than Cu sorbed to birnessite. The latter value is substantially greater than the observed fractionation factor between ferromanganese crusts and seawater which is ~ -0.3 ‰, but both studies confirm that Cu isotope fractionation during adsorption occurs in opposite direction to Zn isotope fractionation. Hence, the concomitant shifts in Cu and Zn isotope compositions in the same direction occurring ca. 6-4 Ma in the South Pacific Fe-Mn crusts cannot be explained by simple sorption-desorption processes associated with, for example, changes of growth rates or post-depositional processes. Cu/Mn and Zn/Mn ratios in South Pacific Fe-Mn crusts show a slight decrease with decreasing time (Figure 1), thus Cu/Mn and Zn/Mn decreases with increasing $\delta^{65/63}Cu_{NIST976}$ and $\delta^{66/64}Zn_{JMC\text{-}Lyon}$ values. By contrast, large variations in Cu/Mn and Zn/Mn ratios observed in North Pacific Fe-Mn crusts are not associated with any significant Cu and Zn isotope variations, thus this likely precludes the effect of a mineralogical control on Cu and Zn isotope fractionation. We further estimated the potential effect of Fe-Mn crust growth on the isotopic composition using Co concentrations

normalized to Mn in Fe-Mn crusts. Cobalt is commonly used for dating Fe-Mn crusts and nodules layers because the flux of Co to the oceans is assumed to be constant through time (Halbach et al., 1983; Puteanus and Halbach, 1988), and thus variations in Co/Mn ratios of the crust would reflect variations in growth rate of the different layers of the crust. The absence of clear co-variations between Co/Mn ratios and $\delta^{66/64}Zn_{JMC\text{-}Lyon}$ and $\delta^{65/63}Cu_{NIST976}$ in South Pacific Fe-Mn crusts (Table 1) likely suggests that growth rates are not a factor controlling Cu and Zn isotope fractionation. We therefore suggest that the positive correlation observed between $\delta^{65/63}Cu_{NIST976}$ and $\delta^{66/64}Zn_{JMC\text{-}Lyon}$ reflects variable composition of deep seawater rather than in-situ processes, such as adsorption, precipitation or effect of the mineralogy in Fe-Mn crusts.

Because changes in $\delta^{66/64}Zn_{JMC\text{-}Lyon}$ and $\delta^{65/63}Cu_{NIST976}$ recorded in South Pacific crusts occur within an age window of 4 to 6 Ma, which is not recorded in North Pacific crusts, we speculate that regional, rather than global oceanographic events affected deep seawater composition. Figure 4 shows that high Cu/Zn ratios (from 0.97 to 2.33) in both South Pacific Fe-Mn crusts are correlated with light Cu and Zn isotope compositions. North Pacific Fe-Mn crusts display a similar range of Cu/Zn ratio (and even higher ratios) than South Pacific Fe-Mn crusts but do not display any co-variations with isotopic compositions. In fact, decreasing Cu/Zn ratios with time are observed in North Pacific Fe-Mn crusts but they are not contemporaneous to any Cu and Zn isotope variations. The correlation observed between Cu/Zn ratios and Cu and Zn isotope compositions in South Pacific crusts suggests mixing between two end-members with different Cu/Zn ratios and isotopic compositions.

In the following discussion, we evaluate the possible factors resulting in variations of Cu and Zn isotope signatures in the deep Pacific Ocean seawater. Because most Cu and Zn isotope variations occur in the first ~500 m depth, we first evaluate the influence of biogeochemical processes occurring in the water column such as, bioproductivity in surface

371 waters, influence of oxygen minimum areas, continental runoff and continental margin inputs,
372 and volcanic activity and associated hydrothermal inputs; and the impacts of these processes
373 on the deep Pacific Ocean seawater. Then, we compare the results observed in our Fe-Mn
374 crusts with other Fe-Mn deposits, and conclude the discussion by evaluating the impact of our
375 findings on the global oceanic Cu and Zn budgets.
376
377 *4.2. Biogeochemical processes in the water column*
378
379 *4.2.1. Effects of surface bioproductivity and export in deep seawater*
380
381 Zinc is a micronutrient in seawater (Morel and Price, 2003) and it has been shown that
382 Zn isotopes are fractionated during biological uptake with preferential uptake of light Zn
383 isotopes by microorganisms (John et al., 2007; Andersen et al., 2011; Samanta et al., 2017;
384 Köbberich and Vance, 2019). Therefore, one would expect that dissolved Zn in surface
385 seawater is isotopically heavy compared to deep waters. However, this pattern is not
386 systematically observed (e.g., in the Southern Ocean, Zhao et al., 2014). Studies suggest that
387 Zn isotopes in surface waters are dominated by scavenging processes where heavy Zn
388 isotopes are preferentially adsorbed on organic matter resulting in light Zn isotope signatures
389 in seawater (John and Conway, 2014; John et al., 2018; Weber et al., 2018), and intracellular
390 regeneration of light Zn isotopes is also observed in the North Pacific Ocean (Vance et al.,
391 2019). In addition, anthropogenic inputs may also impart light isotope signatures to surface
392 seawaters (Lemaitre et al., 2020; Liao et al., 2020). Thus, suggested relationships between Zn
393 isotopes in the marine geological archive and past paleoproductivity (Pichat et al., 2003;
394 Kunzmann et al., 2013) may in fact be more complex.

In addition, while Zn has clearly a nutrient-type profile in the water column (micronutrient), Cu behavior in the water column is not only affected by biological uptake but also by scavenging and dissolution processes as exemplified by continuous increase in Cu concentrations with depth as a result of dissolution of sinking particles or a benthic flux from sediments (Boyle et al., 1977; Little et al., 2013; Roshan and Wu, 2015; Richon and Tagliabue, 2019). Thus, variations of surface productivity are unlikely to explain the relationships observed between Cu and Zn isotope compositions in the two South Pacific Fe-Mn crusts.

4.2.2. Influence of oxygen minimum areas

Scavenging of trace metals during Mn-oxides colloids formation is probably more efficient at the base of the OMZ (defined as low oxygen concentrations areas, i.e., about 50-100 μM, located between 1000 to 1500 m water depths) due to enhanced oxidation of Mn from the OMZ where dissolved reduced Mn accumulates (Klinkhammer and Bender, 1980; Koschinsky and Halbach, 1995). Thus, Fe-Mn crusts formed close to the OMZ could be preferentially enriched in transition metals in comparison to Fe-Mn crusts precipitated in deeper waters, thus increasing their vertical offset from OMZ depths and resulting in lower Mn/Fe ratios. The subsidence and drift of seamounts during plate motion imply that Fe-Mn crusts have deepened through time, which kept them away from the OMZ. The influence of the depth of OMZ base relatively to the depth of Fe-Mn crusts formation has already been suggested by previous authors to explain highest enrichment in Co, Ni and Mn in the shallowest crusts (Halbach et al., 1984; Aplin and Cronan, 1985; De Carlo et al., 1987). If the location of the crusts relative to the base of an OMZ has varied through time as a consequence of seafloor subsidence and plate motion, so that older parts of the crusts precipitated in

shallower waters were more proximate to the base of an OMZ than their present-day location, then one would expect to have higher Mn/Fe ratios in older part of the crusts (i.e., closer to the rock substrate) than in the younger part (i.e., closer to the crust surface/seawater interface). In fact, an inverse trend is observed in South Pacific Fe-Mn crusts where increasing Mn/Fe ratios are found in the youngest parts of the crusts, suggesting that distance from the OMZ is not responsible for geochemical variations.

Most Zn isotope variations in the water column occur between 0 and ~500 m depth, and more specifically within the first 100 meters depth (Conway and John, 2014; Zhao et al., 2014; Liao et al., 2020), and exhibit lighter values with decreasing depth (Boyle et al., 2012; Vance et al., 2016; John et al., 2018; Vance et al., 2019; Lemaitre et al., 2020). Small Zn isotope variations in the water column are associated with the presence of low oxygen concentrations (< 100 µM), where lighter $\delta^{66/64}Zn_{JMC\text{-}Lyon}$ values are likely related to Zn scavenging onto particles (Conway and John, 2014). However, in deep waters below ~1000 m depth, $\delta^{66/64}Zn_{JMC\text{-}Lyon}$ values remain relatively homogenous in the Pacific Ocean with an average value of ~ 0.5 ‰ (Conway and John, 2015; John et al., 2018; Vance et al., 2019). Copper isotopes are not affected by low oxygen conditions associated with an OMZ and most Cu isotope variations occur in surface waters well above 500 meters depth (Takano et al., 2014), implying that Cu isotope compositions in deep waters (>1000 m depth) should also be homogenous in the Pacific Ocean. Thus, for both Cu and Zn most isotopic variations in the water column occur above 1000 m water depth. This feature is important to highlight because the four crusts studied here are located below the limit where Cu and Zn isotope variations were observed in the water column (1826 and 1530 m for ZEP2-DR05-04 and ZEP2-DR06-03 respectively, and ~2000 and 2079 m for J2-480 and J2-480-R14 respectively) and below the depth of the OMZ. Recording an isotopic signal in Fe-Mn crusts related to processes occurring in the OMZ would require transport of Cu and Zn from the OMZ to deep waters,

for example, via sinking particles. However, this process remains speculative since we cannot demonstrate it with our study. Therefore, the influence of OMZs on elemental composition and Cu and Zn isotope composition of Fe-Mn crusts is not a relevant explanation to the positive correlation observed, but a change in local or global Cu and Zn sources to the oceans, or change in water mass composition is most likely.

4.2.3. Inputs from continental runoff and continental margins

Continental runoff via riverine inputs and atmospheric particles is the main source of dissolved Cu and Zn to seawater (Little et al., 2014). Conway and John (2014) also identified a sedimentary margin Zn source in seawater samples collected near the North American and Iberian margins, while Lemaitre et al. (2020) observed a light Zn benthic source in the North Atlantic Ocean. In the Northwestern Pacific Ocean, light $\delta^{66/64}Zn_{JMC\text{-}Lyon}$ values in deep seawater are also attributed to benthic input of Zn (Liao et al., 2020). Conway and John (2014) show that continental margins are a source of isotopically light Zn with $\delta^{66/64}Zn_{JMC\text{-}Lyon}$ values between ~ -0.7 ‰ and ~ -0.5 ‰ for the Iberian and North American margins respectively. The authors proposed two explanations for this isotopically light Zn source, (1) release of Zn in the sediment during phytoplankton degradation, or (2) release of Zn in the sediment from sulfides formed in the water column. They also suggest that this sedimentary source could be a sink for isotopically light Zn in environments where, for example, Zn is retained in sulfidic or reducing porewaters instead of being released in the water column. This interpretation was also further proposed by Little et al. (2016). A significant source of sedimentary Cu from continental margins has not been clearly demonstrated yet, and the isotope composition of this flux also remains unclear (Little et al., 2017). But the lithogenic Cu has an isotope composition of ~ 0 - 0.1 ‰ (Little et al., 2017), thus lighter than average

seawater Cu isotope composition and lighter than the oldest Fe-Mn crust end-member. The benthic flux have been hypothesized to be a source of dissolved Cu to the deep ocean (Boyle et al., 1977; Roshan and Wu, 2015), but the Cu isotope composition of this flux is not known yet.

The four Fe-Mn crusts investigated here are located a few thousands of kilometers away from continental margins. This would imply either transport of this sedimentary source to the deep ocean or that the crusts were located closer to the continents some time during their growth. The latter could possibly be consistent with lighter Zn isotope composition recorded in the older part of Fe-Mn crusts. The position of Fe-Mn crusts formed in the Pacific Ocean has varied through time in a northwestward direction during plate motion (Meynadier et al., 2008), in which case the position of the crusts relatively to the continents surrounding the Pacific Ocean may have changed. However, based on the model of Meynadier et al. (2008) South Pacific Fe-Mn crusts would have moved from a distance of < 400 km. This distance is too small to consider that Fe-Mn crusts formed close to the continents in their early growth and would have been directly impacted by inputs from continental margins.

4.2.4. Impact of volcanic activity and hydrothermal fluxes in the Pacific Ocean

A study showed that interaction of seawater with fresh lava flows released isotopically light Cu (~ -1.6 ‰) and Zn (~ -0.1‰) in seawater from the basalts (Hawco et al., 2020). The Society Islands exhibit an age progression to the West from Mehetia (less than 1 Ma) to Tahiti (0.6–1.2 Ma), Moorea (1.5–2.0 Ma) Bora Bora (3.1–3.5 Ma) and Maupiti (3.9–4.5 Ma) (Blais et al., 2002; Yamamoto et al., 2002; Uto et al., 2007). The Marquesas Archipelago is the northernmost linear volcanic chain in French Polynesia. It comprises eight main islands and a few islets and seamounts formed between 5.5 and 0.4 Ma (Legendre et al., 2006). By

comparison, the Hawaiian Islands are all younger than 5.1 Ma, with most recent volcanism less than 1 Ma, but most of the older islands have since subsided below sea level. This indicates that the timing of regional volcanic activity (i.e., volcanic seamounts are younger than 6 Ma) is not consistent with the observed Fe-Mn crusts Cu and Zn isotope patterns (i.e., light Cu and Zn isotope compositions are older than 6 Ma). Hence, it does not seem that regional hotspot-related volcanic activity affects Fe-Mn crusts composition. In particular, the formation of Society Islands and Marquesas marked a period of less than 5.5 Ma, which is associated with Cu and Zn isotope signatures consistent with modern deep seawater. The volcanic chain extending from the Rurutu Island and nearby seamounts was dated at 12 Ma (Clouard and Bonneville, 2001). Hence, it is unlikely that low $\delta^{66/64}Zn_{JMC\text{-}Lyon}$-$\delta^{65/63}Cu_{NIST976}$ end-members, located at the base of the Fe-Mn crusts are affected by the latest stages of the formation of the volcanic seamounts nearby Rurutu Island and to the weathering of fresh lava flows.

The influence of hydrothermal activity on transition metal enrichment in South Eastern Pacific sediments was first mentioned by Boström et al. (1969). Although most transition metals delivered by hydrothermal fluids are precipitated in the vicinity of vent sites, a significant proportion of Cu and Fe, for example, may enter the deep ocean through complexation with organic ligands (Coale and Bruland, 1988; Toner et al., 2009; Sander and Koschinsky, 2011; Resing et al., 2015). Hannington (2013) recently highlighted that accumulation of Cu in South Pacific deep-sea sediments through time may exceed the total amount of Cu deposited at ridge axis. Modelling of Cu transport from hydrothermal vents by complexation with organic ligands may account for 14% of the Cu dissolved in seawater (Sander and Koschinsky, 2011), especially in ultramafic-hosted hydrothermal sites where abiotic production of organic compounds is enhanced. Nevertheless, measurements of dissolved Cu near hydrothermal sources yield contrasted results. Seawater samples from the

GA03 transect in the North Atlantic indicate removal of Cu near the TAG hydrothermal vent (Roshan and Wu, 2015). Copper concentrations in seawater at the EPR in the South Pacific does not show any removal nor increase in dissolved Cu, but an increase in particulate Cu just above hydrothermal sources is observed (GEOTRACES Intermediate Data Product Group, 2021). Therefore, how Cu can be transported over long distances from the ridge-axis remains unclear to date and must be investigated in the future. Transport of hydrothermal Zn in seawater on long distance of thousands of kilometers has been demonstrated in the South Pacific Ocean (Roshan et al., 2016; John et al., 2018) and in the North Atlantic Ocean (Conway and John, 2014; Lemaitre et al., 2020). Organic complexation of Zn from hydrothermal fluids is not specifically documented in the literature, but it was demonstrated that Zn forms strong organic ligands in seawater (e.g., Mackey, 1983; Bruland, 1989; Donat and Bruland, 1990; Ellwood and Van den Berg, 2000; Kim et al., 2015), or that it could be transported as Zn sulphide nanoparticulates (Conway and John, 2014).

The Tahiti archipelago, where the South Pacific Fe-Mn crusts were collected, is clearly within the area of the Pacific Ocean (between 10-20°S) characterized by large-scale ^{3}He enrichment at 2500 m depth (Lupton and Craig, 1981; Lupton, 1995; Urabe et al., 1995). One can suggest that, for a long period of time, the South Pacific area has been receiving large hydrothermal inputs from the superfast East Pacific Rise (EPR) segments (Resing et al., 2015). Local hydrothermal sources have been also proposed, for example through active volcanic seamounts such as Teahitia potentially associated with reactivation of the Society Islands Hotspots (German et al., 2020). Hence, we interpret the difference in Cu and Zn isotope records between the South Pacific and the North Pacific Fe-Mn crusts as being related to local contribution of trace metals from hydrothermal sources that would have affected water masses of the South Pacific Ocean from more than 6 Ma ago until 4 Ma.

The effect of hydrothermal Zn on the deep seawater Zn have been directly observed in the Atlantic Ocean where $\delta^{66/64}Zn_{JMC\text{-}Lyon}$ values of ~ -0.5 ‰ have been measured in deep waters near TAG hydrothermal vent in comparison with the average value of ~ 0.5 ‰ for deep waters (Conway and John, 2014; John et al., 2018). In addition, light Zn isotopes (~ -0.3 ‰) measured in seawater near the Reykjanes Ridge was attributed to hydrothermal inputs transported by the Labrador Sea Water from the MAR (Mid-Atlantic Ridge) over 1000 km (Lemaitre et al., 2020). The authors calculated a hydrothermal end-member of ~ -0.5 ‰ responsible for lighter Zn isotopes values (Lemaitre et al., 2020), which is consistent with the value of ~ -0.5 ‰ measured near the TAG hydrothermal field (Conway and John, 2014). However, in the Pacific Ocean, Zn in hydrothermal fluids from EPR hydrothermal vent sites is enriched in heavy isotopes from 0.0 ‰ to 1.0 ‰ relatively to the source rock as a result of precipitation of isotopically light Zn in sulfides (John et al., 2008). In other words, high temperature hydrothermal vents have probably Zn isotope values close to basalt values, but when fluids cool and sulfides precipitate, the fluids become enriched in isotopically heavy Zn. John et al. (2018) calculated the Zn isotope composition of a hydrothermal end-member in South Pacific seawater of ~ 0.2 ‰. The authors argued that hydrothermal fluids might possibly affect Zn isotopes budget of seawater, but notably the Zn isotope composition of the Pacific Ocean hydrothermal end-member is significantly heavier than the average value calculated for the Atlantic Ocean (~ -0.5 ‰). Copper isotope composition of hydrothermal fluids has been recently reported in the literature and suggests slightly heavier values (i.e., ~ 0-0.4 ‰) than basaltic values for high-temperature hydrothermal fluid end-members, although heavier $\delta^{65/63}Cu_{NIST976}$ have been also reported in vent fluids (i.e., ~ 1.1 ‰, Syverson et al., 2021) and active hydrothermal chimneys (i.e., up to ~ 3 ‰, Rouxel et al., 2004).

In our Figure 3, taking a hydrothermal end-member for the South Pacific seawater (lower end of the trend) with values of ~ 0.2 ‰ for $\delta^{65/63}Cu_{NIST976}$ and ~ 0.7 ‰ for $\delta^{66/64}Zn_{JMC\text{-}}$

569 $_{Lyon}$, and a "Pacific seawater" end-member represented by the average North Pacific Fe-Mn
570 crusts ($\delta^{65/63}Cu_{NIST976}$ ~ 0.7 ‰ and $\delta^{66/64}Zn_{JMC\text{-}Lyon}$ ~ 1.2 ‰), we can reconstruct the seawater
571 isotope composition using Cu and Zn isotope fractionation factors between Fe-Mn crusts and
572 seawater of -0.3 ‰ and 0.5 ‰ respectively. This yields a Pacific seawater with $\delta^{65/63}Cu_{NIST976}$
573 ~ 1 ‰ and $\delta^{66/64}Zn_{JMC\text{-}Lyon}$ ~ 0.7 ‰, and a hydrothermal fluid end-member with $\delta^{65/63}Cu_{NIST976}$
574 ~ 0.5 ‰ and $\delta^{66/64}Zn_{JMC\text{-}Lyon}$ ~ 0.2 ‰. These values are slightly offset from the average
575 modern seawater values (0.7 ‰ for Cu, and 0.5 ‰ for Zn) and from known values for Pacific
576 hydrothermal fluids (0-0.4 ‰ for Cu, and 0.2 ‰ for Zn). Possible reasons are the uncertainty
577 in the determination of the Cu and Zn isotope compositions of Pacific hydrothermal fluids and
578 the fractionation factors between seawater and ferromanganese crusts.
579 Despite these uncertainties, the trend observed in Figure 3 is consistent with the fact
580 that the source of Cu and Zn in the older Fe-Mn crusts tends towards a source end-member
581 dominated by hydrothermal inputs. We interpret the results shown by South Pacific Fe-Mn
582 crusts as the result of sustained hydrothermal influence from the EPR during the early stages
583 of Fe-Mn crust formations, 4-6 Ma ago.
584
585 *4.3. Comparison with other oceanic Fe-Mn deposits*
586
587 High Cu/Zn ratios (between ~2 and ~4) were also reported for Bauer Basin Fe-Mn
588 crusts, yet these Fe-Mn oxide deposits (including Fe-Mn crusts and nodules) are known to
589 have been affected by disseminated hydrothermal particles remaining in the water column
590 after inputs from the EPR that did not precipitate near the vent (Elderfield and Greaves,
591 1981). Therefore, increasing Cu/Zn ratios correlating with decreasing $\delta^{65/63}Cu_{NIST976}$ and
592 $\delta^{66/64}Zn_{JMC\text{-}Lyon}$ in South Pacific Fe-Mn crusts is consistent with hydrothermal inputs in
593 seawater.

As illustrated in Figure 3, Cu and Zn isotope composition of Fe-Mn crusts and nodules from different oceanic basins do not all plot on the linear trend defined by North and South Pacific Fe-Mn crusts. Mn-nodules show more scatter in $\delta^{66/64}Zn_{JMC\text{-}Lyon}$ - $\delta^{65/63}Cu_{NIST976}$ relationships because they are probably influenced by diagenetic processes and metal cycling occurring in sediment porewaters. Hence, the isotope composition of the surface scrapings of nodules reported by Maréchal et al. (2000) and Albarède (2004) are not accurate proxies of seawater isotopic composition through time. The dataset shown in Figure 3 also includes isotopic compositions of bulk Fe-Mn crusts samples which composition represents an average of the composition through time. Little et al. (2014) found no variations through time in the Cu and Zn isotope compositions of the three Fe-Mn crusts from the Atlantic, Indian and Pacific Oceans. If we look at Figure 3, one can see that most Fe-Mn crusts samples from the Central Pacific Ocean (Little et al., 2014) (located Southwestern of the North Pacific Fe-Mn crusts from this study) plot in the trend defined by our Fe-Mn crusts time-series, and are all very close to the Pacific seawater end-member. Outlier samples with lighter (-0.16 ‰) and heavier (1.19 ‰) $\delta^{65/63}Cu_{NIST976}$ values, and lighter (0.60 ‰) and heavier (1.42 ‰) $\delta^{66/64}Zn_{JMC\text{-}Lyon}$ value reported for the Indian Fe-Mn crust by Little et al. (2014) were interpreted as the result of a lower enrichment in Cu or Zn in the Fe-Mn crusts, implying that the Cu and Zn isotopic signal in the Fe-Mn phases could have been biased by the presence of other mineral phases in the crust.

4.4. Implication for global Cu and Zn isotope budget

Our results suggest that contribution of hydrothermal inputs as a source of dissolved marine Cu and Zn is significant and could be persistent through time. Little et al. (2014) assumed that rivers are the only important source of marine Cu and Zn. They also pointed out

619 that the mass balance for Zn was not achieved which they attributed to a missing sink. By
620 contrast, there is a missing isotopically light input flux necessary to balance the marine Cu
621 isotopic budget (Little et al., 2017). These missing fluxes could be accounted for by the
622 hydrothermal flux to the oceans of Cu and Zn as recently reevaluated for Zn by Roshan et al.
623 (2016). Our results bolster recent studies arguing for the non-negligible role of
624 hydrothermalism on the oceanic pool of dissolved transition metals such as Fe (Tagliabue et
625 al., 2010; Saito et al., 2013; Horner et al., 2015; Resing et al., 2015) in particular Fe in the
626 South Pacific Ocean (Fitzsimmons et al., 2014), Ni (Gall et al., 2013; Gueguen et al., 2021),
627 Cu (Hannington, 2013) and Zn (Roshan et al., 2016). For instance, Horner et al. (2015) argued
628 that deeply sourced Fe including Fe from hydrothermal venting has a strong influence on the
629 distribution of deep Fe contrasting with previous studies suggesting that oceanic Fe is
630 predominantly supplied by continental aeolian dust and particles. This finding calls into
631 question the effective role of hydrothermal inputs on the global marine biogeochemical
632 cycling of trace metals suggesting that, besides continental sources (rivers and dusts), mass
633 balance of key transition metals in seawater may also be strongly controlled by hydrothermal
634 sources. This picture is particularly relevant for the South Pacific Ocean where hydrothermal
635 venting from the East Pacific Rise has likely a significant influence on the distribution of trace
636 metals in seawater.
637
638 **5. Summary and concluding remarks**
639
640 Copper and Zinc isotope patterns during the last ~17 Ma are distinct for Fe-Mn crusts
641 formed in the North Pacific and those in the South Pacific Ocean. North Pacific Fe-Mn crusts
642 show limited Cu and Zn isotope variations through time with values between 0.57 and 0.73 ‰
643 for $\delta^{65/63}Cu_{NIST976}$ and between 0.97 ‰ to 1.25 ‰ for $\delta^{66/64}Zn_{JMC\text{-}Lyon}$. The range in isotopic

644 variations is larger in South Pacific crusts than in North Pacific crusts with Zn isotopes
645 varying from 0.67 to 1.09 ‰ and Cu isotopes are comprised in the 0.16 - 0.51 ‰ range.
646 The major finding of this study is the positive correlation between $\delta^{65/63}Cu_{NIST976}$
647 values and $\delta^{66/64}Zn_{JMC\text{-}Lyon}$ values in South Pacific Fe-Mn crusts, which has not been observed
648 in Fe-Mn crusts from other oceanic regions (Atlantic, Indian and Antarctic Oceans).
649 Variations are not related to precipitation processes or mineralogical effects, but we interpret
650 these patterns as being the result of hydrothermal inputs from the East Pacific Rise where
651 transport of Cu and Zn with organic ligands or sulphide nanoparticulates may have favored
652 their dispersion in deep seawater. We show that significant hydrothermal inputs 6 Ma ago
653 affected both Cu and Zn isotope compositions in the South Pacific Ocean. The four Fe-Mn
654 crusts investigated here plot along a trend defined by a hydrothermal end-member
655 ($\delta^{65/63}Cu_{NIST976}$ ~ 0.2 ‰ and $\delta^{66/64}Zn_{JMC\text{-}Lyon}$ ~ 0.7‰) and a "Pacific seawater" end-member
656 ($\delta^{65/63}Cu_{NIST976}$ ~ 0.7 ‰ and $\delta^{66/64}Zn_{JMC\text{-}Lyon}$ ~ 1.2 ‰). The values of the end-members are
657 fractionated from seawater by a factor of -0.3 ‰ and 0.5 ‰ for Cu and Zn respectively. Our
658 study further suggests that hydrothermal venting could be an important source of Cu and Zn
659 in seawater, in particular in the South Pacific Ocean, and that it could persist during several
660 million years. Investigation of additional Fe-Mn crusts from other locations in the South
661 Pacific will confirm the extent of hydrothermal influence on the chemical composition of the
662 South Pacific Ocean.
663
664 **Acknowledgments:**
665
666 We thank the FeMO team, K. Edwards, C. Moyer, H. Staudigel, B. Tebo, D. Emerson, and B.
667 Glazer and R/V Kilo Moana and ROV Jason II for facilitating access to samples from Hawaii.
668 We thank Philippe Fernagu (Ifremer Brest, France) for his help during preparation of Fe-Mn

crusts samples for microdrilling. We thank Yoan Germain for his assistance in the clean lab, Emmanuel Ponzevera for his assistance during MC-ICP-MS analyses and Marie-Laure Rouget and Claire Bassoulet for analyses on the ICP-MS. We thank Yazhou Fu, Tim Conway and two anonymous reviewers and for helpful comments on our paper. We also thank the associate editor Susan H. Little and executive editor Jeffrey G. Catalano for very constructive and thorough reviews and additional comments on our manuscript. The study was supported by funding from the European Reintegration grant #FP7 #247837, and the LabexMer ANR-10-LABX-19-01.

Figure captions:

Figure 1: Cu/Mn (panels A and B), Zn/Mn (panels C and D) ratios time-series in South Pacific Fe-Mn crusts and North Pacific Fe-Mn crusts respectively. Cu/Mn and Zn/Mn ratios in South Pacific Fe-Mn crusts show limited temporal variations. Cu/Mn ratios in North Pacific Fe-Mn crusts display a decreasing pattern from older to younger part of the crust whereas the opposite trend is observed for Zn/Mn ratios.

Figure 2: Cu and Zn isotopes (‰) time-series in South Pacific Fe-Mn crusts (panels A and C) and North Pacific Fe-Mn crusts (panels B and D). The latter displays constant Cu and Zn isotope compositions through time whereas similar temporal Cu and Zn isotope variations are observed in both South Pacific Fe-Mn crusts.

Figure 3: Plot showing $\delta^{65/63}Cu_{NIST976}$ versus $\delta^{66/64}Zn_{JMC\text{-}Lyon}$ values (‰) in South Pacific and North Pacific Fe-Mn crusts time-series (large red symbols), smaller red triangles correspond to bulk Fe-Mn crusts. Literature data for Cu and Zn isotope composition in Fe-Mn crusts

(Little et al., 2014) (circles) and nodules (Maréchal et al., 2000; Albarède, 2004) (triangles) is shown by colored symbols. The positive trend displayed by our time-series Fe-Mn crusts (large red symbols) is exemplified by the dotted red line (r^2=0.90). The blue ellipse outlines the cluster of values for North Pacific Fe-Mn crusts which would represent the Pacific seawater end-member of the trend, and the light green box represents the hydrothermal end-member. Mixing between these two end-members could account for the correlation between Cu and Zn isotopes in South Pacific Fe-Mn crusts. Note that these data include both Fe-Mn crusts and nodules (see text for more explanation).

Figure 4: $\delta^{65/63}Cu_{NIST976}$ and $\delta^{66/64}Zn_{JMC\text{-}Lyon}$ values (‰) versus Cu/Zn ratios in South Pacific (A and B) and North Pacific (C and D) Fe-Mn crusts. $\delta^{65/63}Cu_{NIST976}$ and $\delta^{66/64}Zn_{NIST3168a}$ values in North Pacific Fe-Mn crusts do not vary with varying Cu/Zn ratios, whereas South Pacific Fe-Mn crusts display decreasing Cu/Zn ratios with increasing $\delta^{65/63}Cu_{NIST976}$ and $\delta^{66/64}Zn_{JMC\text{-}Lyon}$ values in both Fe-Mn crusts. Higher Cu/Zn ratios with lighter Cu and Zn isotope values are compatible with scattered hydrothermal inputs in the deep South Pacific Ocean.

Table captions:

Table 1: Mn/Fe, Cu/Mn, Zn/Mn and Cu/Zn ratios, and Cu and Zn isotope composition (in ‰) of ferromanganese crusts time-series from the South Pacific, the North Pacific, and bulk ferromanganese crusts from various locations.

References:

Albarède, F. (2004) The Stable Isotope Geochemistry of Copper and Zinc. *Rev. Mineral. Geochem.* **55**, 409-427.

Andersen, M.B., Vance, D., Archer, C., Anderson, R.F., Ellwood, M.J. and Allen, C.S. (2011) The Zn abundance and isotopic composition of diatom frustules, a proxy for Zn availability in ocean surface seawater. *Earth. Planet. Sc. Lett.* **301**, 137-145.

Aplin, A.C. and Cronan, D.S. (1985) Ferromanganese oxide deposits from the Central Pacific ocean. 1. Encrustations from the Line islands archipelago. *Geochim. Cosmochim. Ac.* **49**, 427-436.

Archer, C., Andersen, M.B., Cloquet, C., Conway, T.M., Dong, S., Ellwood, M., Moore, R., Nelson, J., Rehkämper, M., Rouxel, O., Samanta, M., Shin, K.-C., Sohrin, Y., Takano, S. and Wasylenki, L. (2017) Inter-calibration of a proposed new primary reference standard AA-ETH Zn for zinc isotopic analysis. *J. Anal. Atom. Spectrom.* **32**, 415-419.

Baconnais, I., Rouxel, O., Dulaquais, G. and Boye, M. (2019) Determination of the copper isotope composition of seawater revisited: A case study from the Mediterranean Sea. *Chem. Geol.* **511**, 465-480.

Baker, E.T., German, C.R. and Elderfield, H. (1995) Hydrothermal Plumes Over Spreading-Center Axes: Global Distributions and Geological Inferences, *Seafloor Hydrothermal Systems: Physical, Chemical, Biological, and Geological Interactions*. American Geophysical Union, Geophysical Monograph Series, pp. 47-71.

Baker, E.T. and Massoth, G.J. (1986) Hydrothermal Plume Measurements: A Regional Perspective. *Science* **234**, 980-982.

Bermin, J., Vance, D., Archer, C. and Statham, P.J. (2006) The determination of the isotopic composition of Cu and Zn in seawater. *Chem. Geol.* **226**, 280-297.

Bigalke, M., Weyer, S., Kobza, J. and Wilcke, W. (2010) Stable Cu and Zn isotope ratios as tracers of sources and transport of Cu and Zn in contaminated soil. *Geochim. Cosmochim. Ac.* **74**, 6801-6813.

Biller, D.V. and Bruland, K.W. (2012) Analysis of Mn, Fe, Co, Ni, Cu, Zn, Cd, and Pb in seawater using the Nobias-chelate PA1 resin and magnetic sector inductively coupled plasma mass spectrometry (ICP-MS). *Mar. Chem.* **130–131**, 12-20.

Blais, S., Guille, G.r., Guillou, H., Chauvel, C., Maury, R.C., Pernet, G. and Cotten, J. (2002) The island of Maupiti : the oldest emergent volcano in the Society hot spot chain (French Polynesia). *B. Soc. Geol. Fr.* **173**, 45-55.

Bonatti, E., Kraemer, T. and Rydell, H. (1972) Classification and genesis of submarine iron-manganese deposits, *Ferromanganese deposits on the Ocean Floor*, D. Horn ed. Washington DC, Nat. Sci. Found., pp. 149-165.

Boström, K., Peterson, M.N.A., Joensuu, O. and Fisher, D.E. (1969) Aluminum-poor ferromanganoan sediments on active oceanic ridges. *J. Geophys. Res.* **74**, 3261-3270.

Bourles, D., Raisbeck, G.M. and Yiou, F. (1989) ^{10}Be and ^{9}Be in marine sediments and their potential for dating. *Geochim. Cosmochim. Ac.* **53**, 443-452.

Boyle, E.A., John, S., Abouchami, W., Adkins, J.F., Echegoyen-Sanz, Y., Ellwood, M., Flegal, A.R., Fornace, K., Gallon, C., Galer, S., Gault-Ringold, M., Lacan, F., Radic, A., Rehkamper, M., Rouxel, O., Sohrin, Y., Stirling, C., Thompson, C., Vance, D., Xue, Z.C. and Zhao, Y. (2012) GEOTRACES IC1 (BATS) contamination-prone trace element isotopes Cd, Fe, Pb, Zn, Cu, and Mo intercalibration. *Limnol. Oceanogr.* **10**, 653-665.

Boyle, E.A., Sclater, F.R. and Edmond, J.M. (1977) The distribution of dissolved copper in the Pacific. *Earth. Planet. Sc. Lett.* **37**, 38-54.

Bruland, K.W. (1980) Oceanographic distributions of Cadmium, Zinc, Nickel, and Copper in the North Pacific. *Earth. Planet. Sc. Lett.* **47**, 176-198.

Bruland, K.W. (1983) Trace elements in sea water. Academic Press, London.

Bruland, K.W. (1989) Complexation of zinc by natural organic-ligands in the Central North Pacific. *Limnol. Oceanogr.* **34**, 269-285.

Bruland, K.W., Middag, R. and Lohan, M.C. (2014) Controls of Trace Metals in Seawater, in: Holland, H.D., Turekian, K.K. (Eds.), *Treatise on Geochemistry (Second Edition)*. Elsevier, Oxford, pp. 19-51.

Bruland, K.W., Orians, K.J. and Cowen, J.P. (1994) Reactive trace metals in the stratified central North Pacific. *Geochim. Cosmochim. Ac.* **58**, 3171-3182.

Bryan, A.L., Dong, S., Wilkes, E.B. and Wasylenki, L.E. (2015) Zinc isotope fractionation during adsorption onto Mn oxyhydroxide at low and high ionic strength. *Geochim. Cosmochim. Ac.* **157**, 182-197.

Chapman, J.B., Mason, T.F.D., Weiss, D.J., Coles, B.J. and Wilkinson, J.J. (2006) Chemical separation and isotopic variations of Cu and Zn from five geological reference materials. *Geostand. Geoanal. Res.* **30**, 5-16.

Chu, N.C., Johnson, C.M., Beard, B.L., German, C.R., Nesbitt, R.W., Frank, M., Bohn, M., Kubik, P.W., Usui, A. and Graham, I. (2006) Evidence for hydrothermal venting in Fe isotope compositions of the deep Pacific Ocean through time. *Earth. Planet. Sc. Lett.* **245**, 202-217.

Clouard, V.r. and Bonneville, A. (2001) How many Pacific hotspots are fed by deep-mantle plumes? *Geology* **29**, 695-698.

Coale, K.H. and Bruland, K.W. (1988) Copper complexation in the Northeast Pacific. *Limnol. Oceanogr.* **33**, 1084-1101.

Conway, T.M. and John, S.G. (2014) The biogeochemical cycling of zinc and zinc isotopes in the North Atlantic Ocean. *Global. Biogeochem. Cy.* **28**, 1111-1128.

Conway, T.M. and John, S.G. (2015) The cycling of iron, zinc and cadmium in the North East Pacific Ocean – Insights from stable isotopes. *Geochim. Cosmochim. Ac.* **164**, 262-283.

Conway, T.M., Rosenberg, A.D., Adkins, J.F. and John, S.G. (2013) A new method for precise determination of iron, zinc and cadmium stable isotope ratios in seawater by double-spike mass spectrometry. *Anal. Chim. Acta.* **793**, 44-52.

De Carlo, E.H., McMurtry, G.M. and Kim, K.H. (1987) Geochemistry of ferromanganese crusts from the hawaiian archipelago. 1. Northern survey areas. *Deep. Sea. Res.* **34**, 441-467.

Donat, J.R. and Bruland, K.W. (1990) A comparison of two voltammetric techniques for determining zinc speciation in Northeast Pacific Ocean waters. *Mar. Chem.* **28**, 301-323.

Elderfield, H. and Greaves, M.J. (1981) Negative Cerium anomalies in the rare-earth element patterns of oceanic ferromanganese nodules. *Earth. Planet. Sc. Lett.* **55**, 163-170.

Ellwood, M.J. and Van den Berg, C.M.G. (2000) Zinc speciation in the Northeastern Atlantic Ocean. *Mar. Chem.* **68**, 295-306.

Fitzsimmons, J.N., Boyle, E.A. and Jenkins, W.J. (2014) Distal transport of dissolved hydrothermal iron in the deep South Pacific Ocean. *P. Natl. Acad. Sci. USA* **111**, 16654-16661.

Frank, M. (2002) Radiogenic isotopes: Tracers of past ocean circulation and erosional input. *Rev. Geophys.* **40**.

Fu, Y. (2020) Non-traditional stable isotope geochemistry of marine ferromanganese crusts and nodules. *J. Oceanogr.* **76**, 71-89.

Gall, L., Williams, H.M., Siebert, C., Halliday, A.N., Herrington, R.J. and Hein, J.R. (2013) Nickel isotopic compositions of ferromanganese crusts and the constancy of deep ocean inputs and continental weathering effects over the Cenozoic. *Earth. Planet. Sc. Lett.* **375**, 148-155.

German, C.R., Resing, J.A., Xu, G., Yeo, I.A., Walker, S.L., Devey, C.W., Moffett, J.W., Cutter, G.A., Hyvernaud, O. and Reymond, D. (2020) Hydrothermal Activity and Seismicity at Teahitia Seamount: Reactivation of the Society Islands Hotspot? *Frontiers in Marine Science* **7**.

Group, G.I.D.P. (2021) The GEOTRACES Intermediate Data Product 2021 (IDP2021). *NERC EDS British Oceanographic Data Centre NOC*.

Gueguen, B., Rouxel, O. and Fouquet, Y. (2021) Nickel isotopes and rare earth elements systematics in marine hydrogenetic and hydrothermal ferromanganese deposits. *Chem. Geol.* **560**, 119999.

Gueguen, B., Rouxel, O., Rouget, M.-L., Bollinger, C., Ponzevera, E., Germain, Y. and Fouquet, Y. (2016) Comparative geochemistry of four ferromanganese crusts from the Pacific Ocean and significance for the use of Ni isotopes as paleoceanographic tracers. *Geochim. Cosmochim. Ac.* **189**, 214-235.

Halbach, P., Puteanus, D. and Manheim, F.T. (1984) Platinum concentrations in ferromanganese seamount crusts from the Central Pacific. *Naturwissenschaften* **71**, 577-579.

Halbach, P., Segl, M., Puteanus, D. and Mangini, A. (1983) Co-fluxes and growth rates in ferromanganese deposits from Central Pacific seamount areas. *Nature* **304**, 716-719.

Hannington, M.D. (2013) The role of black smokers in the Cu mass balance of the oceanic crust. *Earth. Planet. Sc. Lett.* **374**, 215-226.

Hawco, N.J., Yang, S.-C., Foreman, R.K., Funkey, C.P., Dugenne, M., White, A.E., Wilson, S.T., Kelly, R.L., Bian, X., Huang, K.-F., Karl, D.M. and John, S.G. (2020) Metal isotope signatures from lava-seawater interaction during the 2018 eruption of Kīlauea. *Geochim. Cosmochim. Ac.* **282**, 340-356.

Hein, J.R., Bohrson, W.A., Schulz, M.S., Noble, M. and Clague, D.A. (1992) Variations in the fine-scale composition of a Central Pacific ferromanganese crust: paleoceanographic implications. *Paleoceanography* **7**, 63-77.

Hein, J.R., Conrad, T.A. and Staudigel, H. (2010) Seamount mineral deposits: a source of rare metals for high-technology industries. *Oceanography* **23**, 184-189.

Hein, J.R., Mizell, K., Koschinsky, A. and Conrad, T.A. (2013) Deep-ocean mineral deposits as a source of critical metals for high- and green-technology applications: Comparison with land-based resources. *Ore. Geol. Rev.* **51**, 1-14.

Hein, J.R., Schwab, W.C. and Davis, A.S. (1988) Cobalt-rich and platinum-rich ferromanagenese crusts and associated substrate rocks from the Marshall islands. *Mar. Geol.* **78**, 255-283.

Horner, T.J., Little, S.H., Conway, T.M., Farmer, J.R., Hertzberg, J.E., Janssen, D.J., Lough, A.J.M., McKay, J., Tessin, A., Galer, S.J.G., Jaccard, S.L., Lacan, F., Paytan, A., Wuttig, K. and Members, G.P.B.P.W.G. (2021a) Bioactive trace metals and their isotopes as paleoproductivity proxies: An assessment using GEOTRACES-era data. *Global. Biogeochem. Cy.* **n/a**, e2020GB006814.

Horner, T.J., Little, S.H., Conway, T.M., Farmer, J.R., Hertzberg, J.E., Janssen, D.J., Lough, A.J.M., McKay, J.L., Tessin, A., Galer, S.J.G., Jaccard, S.L., Lacan, F., Paytan, A., Wuttig, K. and Members, G.P.B.P.W.G. (2021b) Bioactive Trace Metals and Their Isotopes as Paleoproductivity Proxies: An Assessment Using GEOTRACES-Era Data. *Global. Biogeochem. Cy.* **35**, e2020GB006814.

Horner, T.J., Schonbachler, M., Rehkämper, M., Nielsen, S.G., Williams, H., Halliday, A.N., Xue, Z. and Hein, J.R. (2010) Ferromanganese crusts as archives of deep water Cd isotope compositions. *Geochem. Geophy. Geosys.* **11**, 1525-2027.

Horner, T.J., Williams, H.M., Hein, J.R., Saito, M.A., Burton, K.W., Halliday, A.N. and Nielsen, S.G. (2015) Persistence of deeply sourced iron in the Pacific Ocean. *P. Natl. Acad. Sci. USA* **112**, 1292-1297.

Ijichi, Y., Ohno, T. and Sakata, S. (2018) Copper isotopic fractionation during adsorption on manganese oxide: Effects of pH and desorption. *GEOCHEMICAL JOURNAL* **52**, e1-e6.

John, S.G. and Conway, T.M. (2014) A role for scavenging in the marine biogeochemical cycling of zinc and zinc isotopes. *Earth. Planet. Sc. Lett.* **394**, 159-167.

John, S.G., Geis, R.W., Saito, M.A. and Boyle, E.A. (2007) Zinc isotope fractionation during high-affinity and low-affinity zinc transport by the marine diatom Thalassiosira oceanica. *Limnol. Oceanogr.* **52**, 2710-2714.

John, S.G., Helgoe, J. and Townsend, E. (2018) Biogeochemical cycling of Zn and Cd and their stable isotopes in the Eastern Tropical South Pacific. *Mar. Chem.* **201**, 256-262.

John, S.G., Rouxel, O.J., Craddock, P.R., Engwall, A.M. and Boyle, E.A. (2008) Zinc stable isotopes in seafloor hydrothermal vent fluids and chinmeys. *Earth. Planet. Sc. Lett.* **269**, 17-28.

Kim, T., Obata, H., Kondo, Y., Ogawa, H. and Gamo, T. (2015) Distribution and speciation of dissolved zinc in the western North Pacific and its adjacent seas. *Mar. Chem.* **173**, 330-341.

Klinkhammer, G.P. and Bender, M.L. (1980) The distribution of manganese in the Pacific Ocean. *Earth. Planet. Sc. Lett.* **46**, 361-384.

Köbberich, M. and Vance, D. (2019) Zn isotope fractionation during uptake into marine phytoplankton: Implications for oceanic zinc isotopes. *Chem. Geol.* **523**, 154-161.

Koschinsky, A. and Halbach, P. (1995) Sequential leaching of marine ferromanganese precipitates: Genetic implications. *Geochim. Cosmochim. Ac.* **59**, 5113-5132.

Koschinsky, A., Stascheit, A., Bau, M. and Halbach, P. (1997) Effects of phosphatization on the geochemical and mineralogical composition of marine ferromanganese crusts. *Geochim. Cosmochim. Ac.* **61**, 4079-4094.

Kunzmann, M., Halverson, G.P., Sossi, P.A., Raub, T.D., Payne, J.L. and Kirby, J. (2013) Zn isotope evidence for immediate resumption of primary productivity after snowball Earth. *Geology* **41**, 27-30.

Legendre, C., Maury, R.C., Blais, S., Guillou, H. and Cotten, J. (2006) Atypical hotspot chains: evidence for a secondary melting zone below the Marquesas (French Polynesia). *Terra Nova* **18**, 210-216.

Lemaitre, N., de Souza, G.F., Archer, C., Wang, R.-M., Planquette, H., Sarthou, G. and Vance, D. (2020) Pervasive sources of isotopically light zinc in the North Atlantic Ocean. *Earth. Planet. Sc. Lett.* **539**, 116216.

Levasseur, S., Frank, M., Hein, J.R. and Halliday, A. (2004) The global variation in the iron isotope composition of marine hydrogenetic ferromanganese deposits: implications for seawater chemistry? *Earth. Planet. Sc. Lett.* **224**, 91-105.

Li, Y.H. and Schoonmaker, J.E. (2003) Chemical Composition and Mineralogy of Marine Sediments, in: Editors-in-Chief: Heinrich, D.H., Karl, K.T. (Eds.), *Treatise on Geochemistry*. Pergamon, Oxford, pp. 1-35.

Liao, W.-H., Takano, S., Yang, S.-C., Huang, K.-F., Sohrin, Y. and Ho, T.-Y. (2020) Zn Isotope Composition in the Water Column of the Northwestern Pacific Ocean: The Importance of External Sources. *Global. Biogeochem. Cy.* **34**, e2019GB006379.

Little, S.H., Archer, C., Milne, A., Schlosser, C., Achterberg, E.P., Lohan, M.C. and Vance, D. (2018) Paired dissolved and particulate phase Cu isotope distributions in the South Atlantic. *Chem. Geol.* **502**, 29-43.

Little, S.H., Sherman, D.M., Vance, D. and Hein, J.R. (2014b) Molecular controls on Cu and Zn isotopic fractionation in Fe–Mn crusts. *Earth. Planet. Sc. Lett.* **396**, 213-222.

Little, S.H., Vance, D., McManus, J. and Severmann, S. (2016) Key role of continental margin sediments in the oceanic mass balance of Zn and Zn isotopes. *Geology* **44**, 207-210.

Little, S.H., Vance, D., McManus, J., Severmann, S. and Lyons, T.W. (2017) Copper isotope signatures in modern marine sediments. *Geochim. Cosmochim. Ac.* **212**, 253-273.

Little, S.H., Vance, D., Siddall, M. and Gasson, E. (2013) A modeling assessment of the role of reversible scavenging in controlling oceanic dissolved Cu and Zn distributions. *Global. Biogeochem. Cy.* **27**, 780-791.

Little, S.H., Vance, D., Walker-Brown, C. and Landing, W.M. (2014) The oceanic mass balance of copper and zinc isotopes, investigated by analysis of their inputs, and outputs to ferromanganese oxide sediments. *Geochim. Cosmochim. Ac.* **125**, 673-693.

Lupton, J. (1998) Hydrothermal helium plumes in the Pacific Ocean. *Journal of Geophysical Research: Oceans* **103**, 15853-15868.

Lupton, J.E. (1995) Hydrothermal Plumes: Near and Far Field, *Seafloor Hydrothermal Systems: Physical, Chemical, Biological, and Geological Interactions*. American Geophysical Union, Geophysical Monograph Series, pp. 317-346.

Lupton, J.E. and Craig, H. (1981) A Major Helium-3 Source at 15°S on the East Pacific Rise. *Science* **214**, 13-18.

Mackey, D.J. (1983) Metal-organic complexes in seawater — An investigation of naturally occurring complexes of Cu, Zn, Fe, Mg, Ni, Cr, Mn and Cd using high-performance liquid chromatography with atomic fluorescence detection. *Mar. Chem.* **13**, 169-180.

Maréchal, C.N., Nicolas, E., Douchet, C. and Albarède, F. (2000) Abundance of zinc isotopes as a marine biogeochemical tracer. *Geochem. Geophys. Geosyst.* **1**, 1-15.

Marechal, C.N., Telouk, P. and Albarede, F. (1999) Precise analysis of copper and zinc isotopic compositions by plasma-source mass spectrometry. *Chem. Geol.* **156**, 251-273.

Meynadier, L., Allegre, C. and O'Nions, R.K. (2008) Plate tectonics, radiogenic isotopic tracers and paleoceanography - The case of the manganese crusts in the Pacific. *Earth. Planet. Sc. Lett.* **272**, 513-522.

Minami, T., Konagaya, W., Zheng, L., Takano, S., Sasaki, M., Murata, R., Nakaguchi, Y. and Sohrin, Y. (2015) An off-line automated preconcentration system with ethylenediaminetriacetate chelating resin for the determination of trace metals in seawater by high-resolution inductively coupled plasma mass spectrometry. *Anal. Chim. Acta.* **854**, 183-190.

Moffett, J.W. and Dupont, C. (2007) Cu complexation by organic ligands in the sub-arctic NW Pacific and Bering Sea. *Deep. Sea. Res. Pt. I.* **54**, 586-595.

Morel, F.M.M. and Price, N.M. (2003) The Biogeochemical Cycles of Trace Metals in the Oceans. *Science* **300**, 944.

Moynier, F., Vance, D., Fujii, T. and Savage, P. (2017) The Isotope Geochemistry of Zinc and Copper. *Rev. Mineral. Geochem.* **82**, 543-600.

Paulmier, A. and Ruiz-Pino, D. (2009) Oxygen minimum zones (OMZs) in the modern ocean. *Prog. Oceanogr.* **80**, 113-128.

Pichat, S., Douchet, C. and Albarède, F. (2003) Zinc isotope variations in deep-sea carbonates from the eastern equatorial Pacific over the last 175 ka. *Earth. Planet. Sc. Lett.* **210**, 167-178.

Puteanus, D. and Halbach, P. (1988) Correlation of Co concentration and growth rate — A method for age determination of ferromanganese crusts. *Chem. Geol.* **69**, 73-85.

Rehkämper, M., Frank, M., Hein, J.R. and Halliday, A. (2004) Cenozoic marine geochemistry of thallium deduced from isotopic studies of ferromanganese crusts and pelagic sediments. *Earth. Planet. Sc. Lett.* **219**, 77-91.

Rehkämper, M., Frank, M., Hein, J.R., Porcelli, D., Halliday, A., Ingri, J. and Liebetrau, V. (2002) Thallium isotope variations in seawater and hydrogenetic, diagenetic, and hydrothermal ferromanganese deposits. *Earth. Planet. Sc. Lett.* **197**, 65-81.

Resing, J.A., Sedwick, P.N., German, C.R., Jenkins, W.J., Moffett, J.W., Sohst, B.M. and Tagliabue, A. (2015) Basin-scale transport of hydrothermal dissolved metals across the South Pacific Ocean. *Nature* **523**, 200-203.

Richon, C. and Tagliabue, A. (2019) Insights Into the Major Processes Driving the Global Distribution of Copper in the Ocean From a Global Model. *Global. Biogeochem. Cy.* **33**, 1594-1610.

Roshan, S. and Wu, J. (2015) The distribution of dissolved copper in the tropical-subtropical north Atlantic across the GEOTRACES GA03 transect. *Mar. Chem.* **176**, 189-198.

Roshan, S., Wu, J. and Jenkins, W.J. (2016) Long-range transport of hydrothermal dissolved Zn in the tropical South Pacific. *Mar. Chem.* **183**, 25-32.

Rouxel, O., Fouquet, Y. and Ludden, J.N. (2004) Copper isotope systematics of the Lucky Strike, Rainbow, and Logatchev sea-floor hydrothermal fields on the Mid-Atlantic Ridge. *Econ. Geol. Bull. Soc.* **99**, 585-600.

Saito, M.A., Noble, A.E., Tagliabue, A., Goepfert, T.J., Lamborg, C.H. and Jenkins, W.J. (2013) Slow-spreading submarine ridges in the South Atlantic as a significant oceanic iron source. *Nature Geosci* **6**, 775-779.

Samanta, M., Ellwood, M.J., Sinoir, M. and Hassler, C.S. (2017) Dissolved zinc isotope cycling in the Tasman Sea, SW Pacific Ocean. *Mar. Chem.* **192**, 1-12.

Sander, S.G. and Koschinsky, A. (2011) Metal flux from hydrothermal vents increased by organic complexation. *Nature. Geosci.* **4**, 145-150.

Schmitt, A.D., Galer, S.J.G. and Abouchami, W. (2009) Mass-dependent cadmium isotopic variations in nature with emphasis on the marine environment. *Earth. Planet. Sc. Lett.* **277**, 262-272.

Segl, M., Mangini, A., Bonani, G., Hofmann, H.J., Nessi, M., Suter, M., Wolfli, W., Friedrich, G., Pluger, W.L., Wiechowski, A. and Beer, J. (1984) ^{10}Be-dating of a manganese crust from Central North Pacific and implications for ocean palaeocirculation. *Nature* **309**, 540-543.

Sherman, D.M. and Little, S.H. (2020) Isotopic disequilibrium of Cu in marine ferromanganese crusts: Evidence from ab initio predictions of Cu isotope fractionation on sorption to birnessite. *Earth. Planet. Sc. Lett.* **549**, 116540.

Sieber, M., Conway, T.M., de Souza, G.F., Hassler, C.S., Ellwood, M.J. and Vance, D. (2020) Cycling of zinc and its isotopes across multiple zones of the Southern Ocean: Insights from the Antarctic Circumnavigation Expedition. *Geochim. Cosmochim. Ac.* **268**, 310-324.

Siebert, C., Nagler, T.F., von Blanckenburg, F. and Kramers, J.D. (2003) Molybdenum isotope records as a potential new proxy for paleoceanography. *Earth. Planet. Sc. Lett.* **211**, 159-171.

Sohrin, Y. and Bruland, K.W. (2011) Global status of trace elements in the ocean. *Trends in Analytical Chemistry* **30**, 1291-1307.

Sohrin, Y., Iwamoto, S., Akiyama, S., Fujita, T., Kugii, T., Obata, H., Nakayama, E., Goda, S., Fujishima, Y., Hasegawa, H., Ueda, K. and Matsui, M. (1998) Determination of trace elements in seawater by fluorinated metal alkoxide glass-immobilized 8-hydroxyquinoline concentration and high-resolution inductively coupled plasma mass spectrometry detection. *Anal. Chim. Acta.* **363**, 11-19.

Sohrin, Y., Urushihara, S., Nakatsuka, S., Kono, T., Higo, E., Minami, T., Norisuye, K. and Umetani, S. (2008) Multielemental determination of GEOTRACES key trace metals in seawater by ICPMS after preconcentration using an ethylenediaminetriacetic acid chelating resin. *Anal. Chem.* **80**, 6267-6273.

Syverson, D.D., Borrok, D.M., Niebuhr, S. and Seyfried, W.E. (2021) Chalcopyrite-dissolved Cu isotope exchange at hydrothermal conditions: Experimental constraints at 350 °C and 50 MPa. *Geochim. Cosmochim. Ac.* **298**, 191-206.

Tagliabue, A., Bopp, L., Dutay, J.C., Bowie, A.R., Chever, F., Jean-Baptiste, P., Bucciarelli, E., Lannuzel, D., Remenyi, T., Sarthou, G., Aumont, O., Gehlen, M. and Jeandel, C. (2010) Hydrothermal contribution to the oceanic dissolved iron inventory. *Nature. Geosci.* **3**, 252-256.

Takano, S., Tanimizu, M., Hirata, T., Shin, K.-C., Fukami, Y., Suzuki, K. and Sohrin, Y. (2017) A simple and rapid method for isotopic analysis of nickel, copper, and zinc in seawater using chelating extraction and anion exchange. *Anal. Chim. Acta.* **967**, 1-11.

Takano, S., Tanimizu, M., Hirata, T. and Sohrin, Y. (2013) Determination of isotopic composition of dissolved copper in seawater by multi-collector inductively coupled plasma mass spectrometry after pre-concentration using an ethylenediaminetriacetic acid chelating resin. *Anal. Chim. Acta.* **784**, 33-41.

Takano, S., Tanimizu, M., Hirata, T. and Sohrin, Y. (2014) Isotopic constraints on biogeochemical cycling of copper in the ocean. *Nature. Com.* **5**, 5663.

Toner, B.M., Fakra, S.C., Manganini, S.J., Santelli, C.M., Marcus, M.A., Moffett, J., Rouxel, O., German, C.R. and Edwards, K.J. (2009) Preservation of iron(II) by carbon-rich matrices in a hydrothermal plume. *Nature. Geosci.* **2**, 197-201.

Urabe, T., Baker, E.T., Ishibashi, J., Feely, R.A., Marumo, K., Massoth, G.J., Maruyama, A., Shitashima, K., Okamura, K., Lupton, J.E., Sonoda, A., Yamazaki, T., Aoki, M., Gendron, J., Greene, R., Kaiho, Y., Kisimoto, K., Lebon, G., Matsumoto, T., Nakamura, K., Nishizawa, A., Okano, O., Paradis, G., Roe, K., Shibata, T., Tennant, D., Vance, T., Walker, S.L., Yabuki, T. and Ytow, N. (1995) The Effect of Magmatic Activity on Hydrothermal Venting Along the Superfast-Spreading East Pacific Rise. *Science* **269**, 1092-1095.

Uto, K., Yamamoto, Y., Sudo, M., Uchiumi, S., Ishizuka, O., Kogiso, T. and Tsunakawa, H. (2007) New K-Ar ages of the Society Islands, French Polynesia, and implications for the Society hotspot feature. *Earth. Planets. Space.* **59**, 879-885.

Vance, D., Archer, C., Bermin, J., Perkins, J., Statham, P.J., Lohan, M.C., Ellwood, M.J. and Mills, R.A. (2008) The copper isotope geochemistry of rivers and the oceans. *Earth. Planet. Sc. Lett.* **274**, 204-213.

Vance, D., de Souza, G.F., Zhao, Y., Cullen, J.T. and Lohan, M.C. (2019) The relationship between zinc, its isotopes, and the major nutrients in the North-East Pacific. *Earth. Planet. Sc. Lett.* **525**, 115748.

Vance, D., Little, S.H., Archer, C., Cameron, V., Andersen, M.B., Rijkenberg, M.J.A. and Lyons, T.W. (2016) The oceanic budgets of nickel and zinc isotopes: the importance of sulfidic environments as illustrated by the Black Sea. *Philos. T. R. Soc. A.* **374**.

Vance, D., Little, Susan H., de Souza, Gregory F., Khatiwala, S., Lohan, Maeve C. and Middag, R. (2017) Silicon and zinc biogeochemical cycles coupled through the Southern Ocean. *Nature. Geosci.* **10**, 202-206.

Weber, T., John, S., Tagliabue, A. and DeVries, T. (2018) Biological uptake and reversible scavenging of zinc in the global ocean. *Science* **361**, 72-76.

Yamamoto, Y., Shimura, K., Tsunakawa, H., Kogiso, T., Uto, K., Barsczus, H.G., Oda, H., Yamazaki, T. and Kikawa, E. (2002) Geomagnetic paleosecular variation for the past 5 Ma in the Society Islands, French Polynesia. *Earth. Planets. Space.* **54**, 797-802.

Yang, S.-C., Hawco, N.J., Pinedo-González, P., Bian, X., Huang, K.-F., Zhang, R. and John, S.G. (2020) A new purification method for Ni and Cu stable isotopes in seawater provides evidence for widespread Ni isotope fractionation by phytoplankton in the North Pacific. *Chem. Geol.* **547**, 119662.

Zhao, Y., Vance, D., Abouchami, W. and de Baar, H.J.W. (2014) Biogeochemical cycling of zinc and its isotopes in the Southern Ocean. *Geochim. Cosmochim. Ac.* **125**, 653-672.

Zhu, X.K., Guo, Y., Williams, R.J.P., O'Nions, R.K., Matthews, A., Belshaw, N.S., Canters, G.W., de Waal, E.C., Weser, U., Burgess, B.K. and Salvato, B. (2002) Mass fractionation processes of transition metal isotopes. *Earth. Planet. Sc. Lett.* **200**, 47-62.

Zhu, X.K., O'Nions, R.K., Guo, Y.L. and Reynolds, B.C. (2000) Secular variation of iron isotopes in North Atlantic Deep Water. *Science* **287**, 2000-2002.

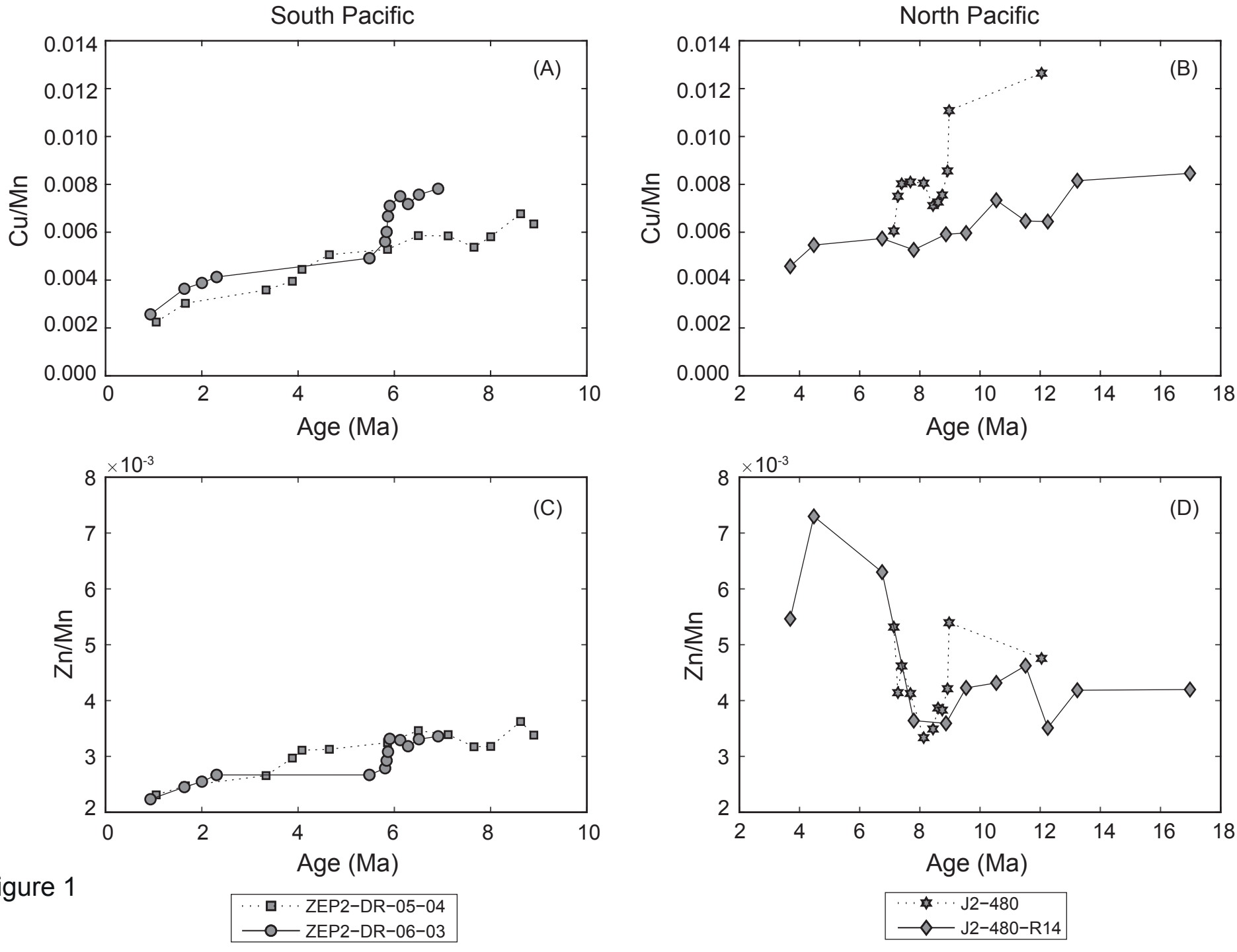
South Pacific
North Pacific
(A)
(B)
(C)
(D)
Cu/Mn
Zn/Mn
Age (Ma)
×10-3
ZEP2-DR-05-04
ZEP2-DR-06-03
J2-480
J2-480-R14

Figure 1

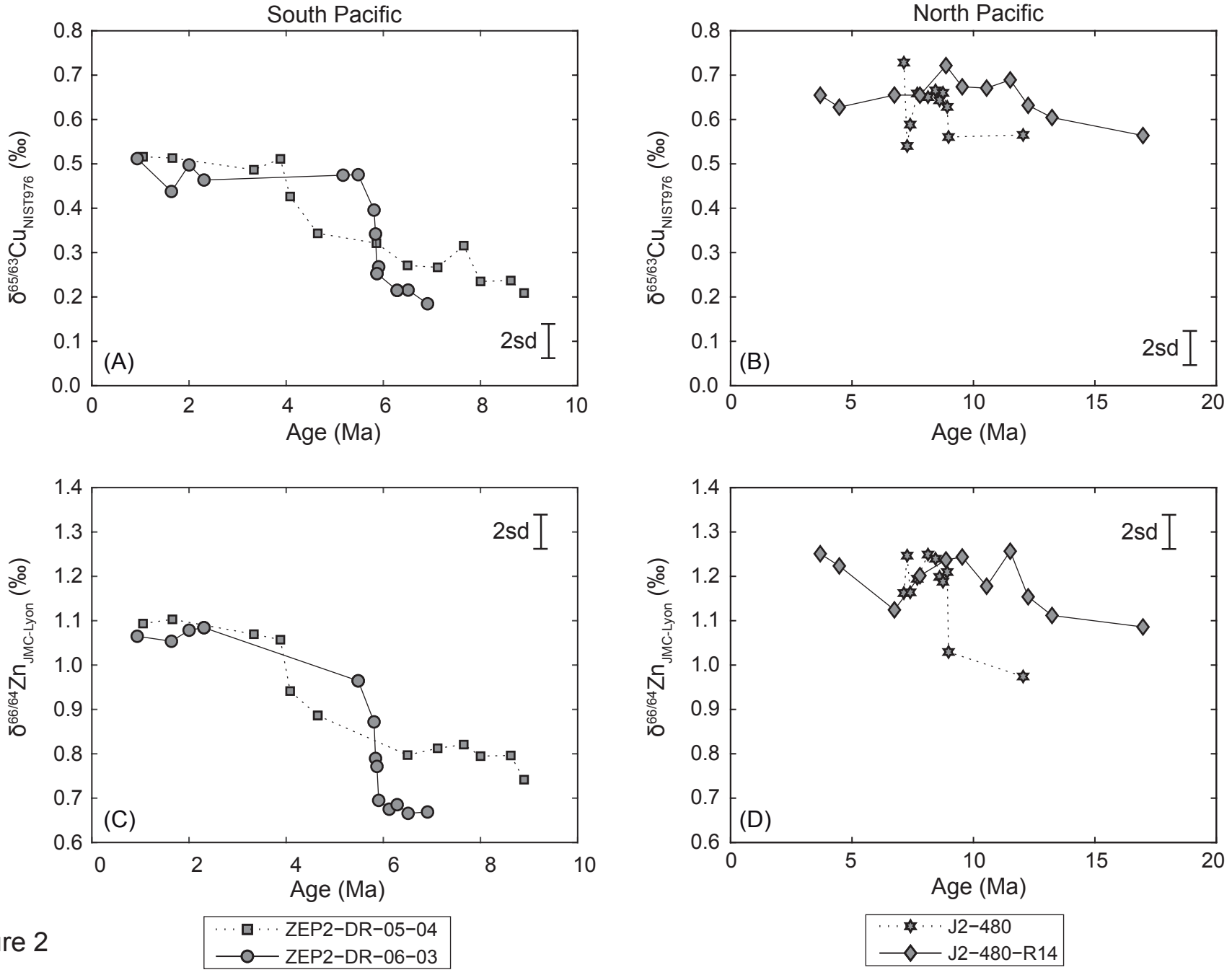
South Pacific
North Pacific
δ65/63CuNIST976 (‰)
Age (Ma)
2sd
(A)
(B)
δ66/64ZnJMC-Lyon (‰)
(C)
(D)
ZEP2-DR-05-04
ZEP2-DR-06-03
J2-480
J2-480-R14

Figure 2

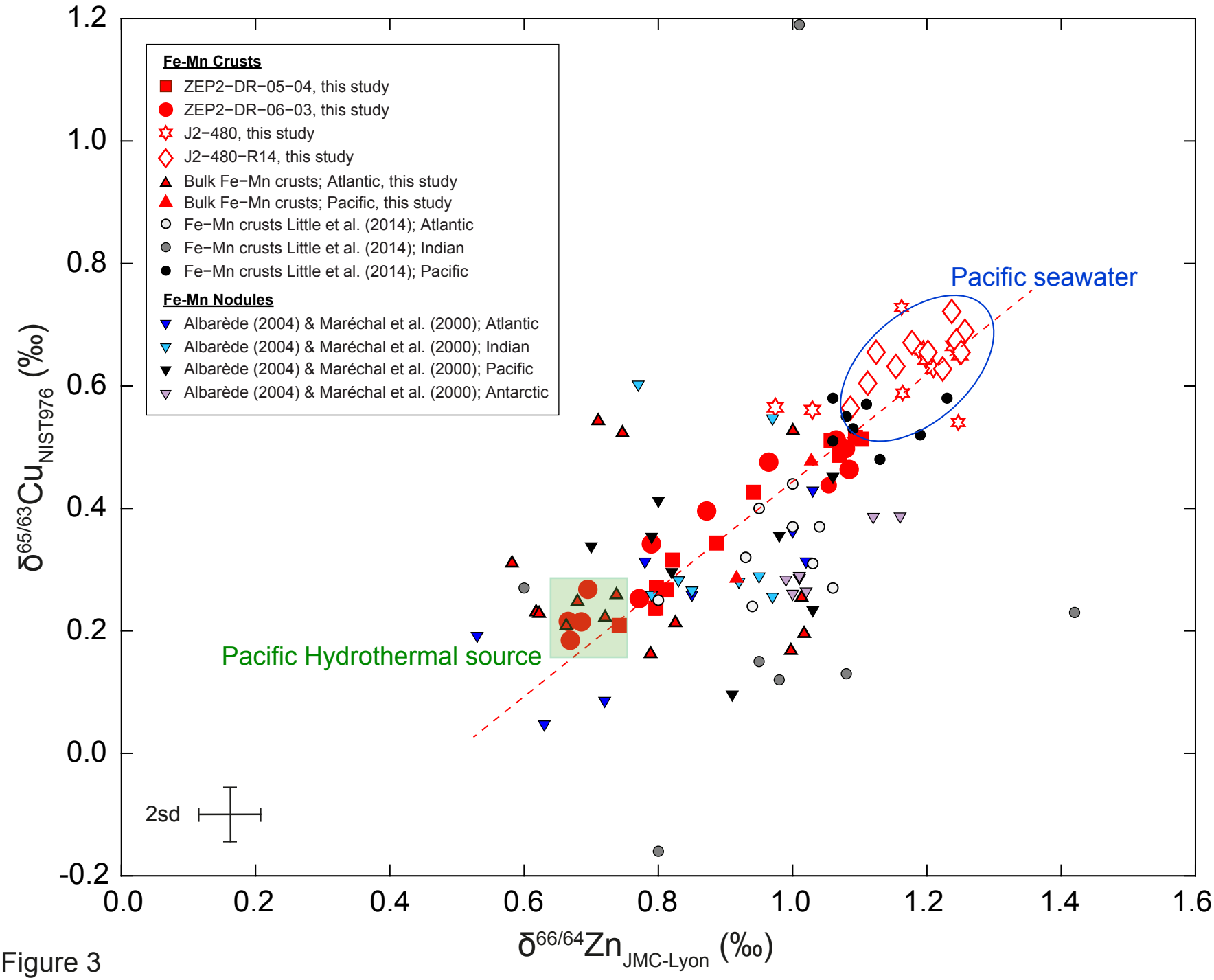
Fe-Mn Crusts
ZEP2-DR-05-04, this study
ZEP2-DR-06-03, this study
J2-480, this study
J2-480-R14, this study
Bulk Fe-Mn crusts; Atlantic, this study
Bulk Fe-Mn crusts; Pacific, this study
Fe-Mn crusts Little et al. (2014); Atlantic
Fe-Mn crusts Little et al. (2014); Indian
Fe-Mn crusts Little et al. (2014); Pacific
Fe-Mn Nodules
Albarède (2004) & Maréchal et al. (2000); Atlantic
Albarède (2004) & Maréchal et al. (2000); Indian
Albarède (2004) & Maréchal et al. (2000); Pacific
Albarède (2004) & Maréchal et al. (2000); Antarctic
Pacific seawater
Pacific Hydrothermal source
2sd
δ65/63CuNIST976 (‰)
δ66/64ZnJMC-Lyon (‰)
1.2
1.0
0.8
0.6
0.4
0.2
0.0
-0.2
0.0
0.2
0.4
0.6
0.8
1.0
1.2
1.4
1.6

Figure 3

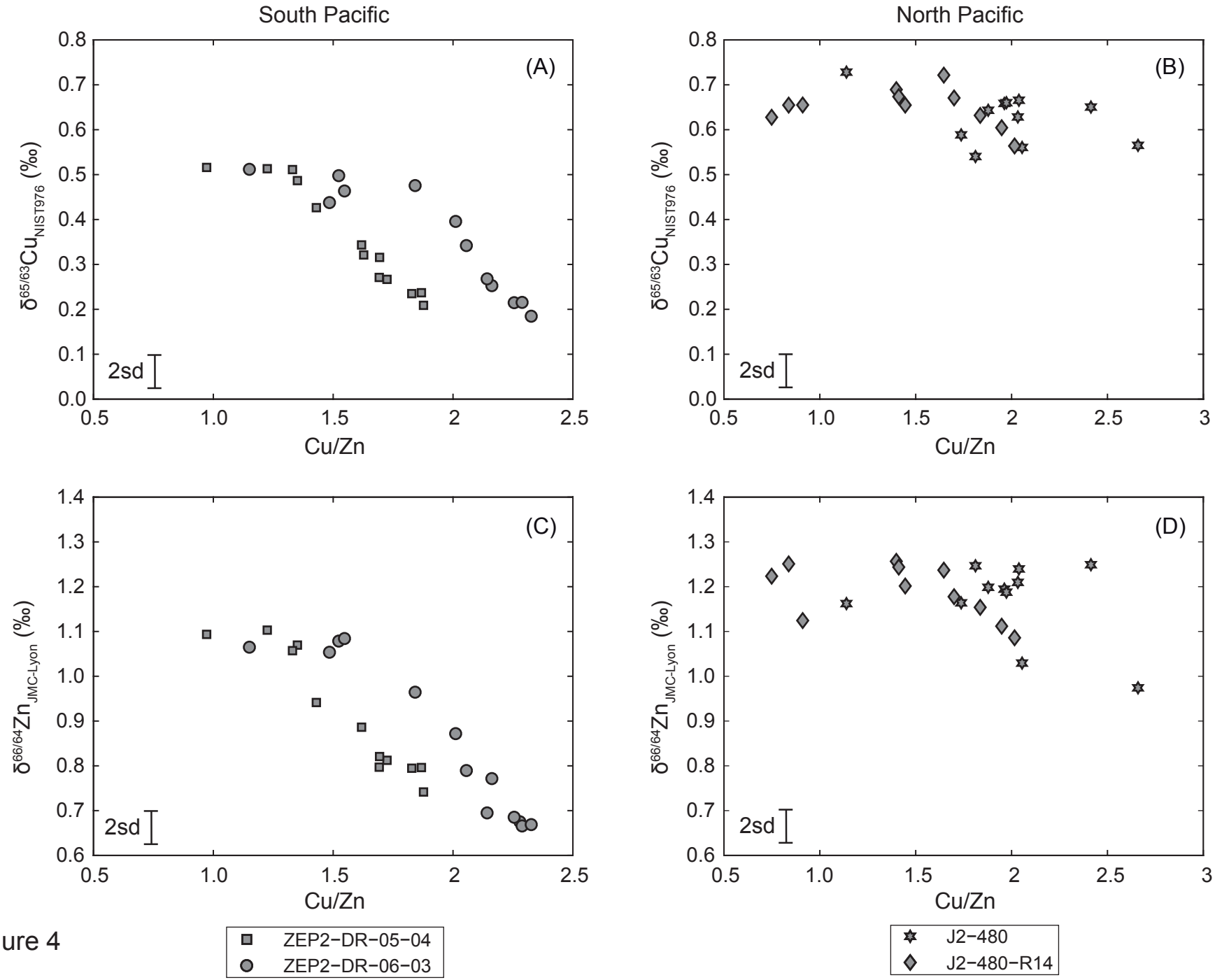
South Pacific
North Pacific
(A)
(B)
(C)
(D)
$\delta^{65/63}Cu_{NIST976}$ (‰)
$\delta^{66/64}Zn_{JMC-Lyon}$ (‰)
Cu/Zn
2sd
ZEP2-DR-05-04
ZEP2-DR-06-03
J2-480
J2-480-R14

Figure 4

Table 1: Mn/Fe, Cu/Mn, Zn/Mn, Cu/Zn and Co/Mn ratios (µg/µg), and Cu and Zn isotopes (‰) in ferromanganese crusts time-series from South Pacific and North Pacific, and bulk Fe-Mn crusts.

Sample name	Location	Depth (mm) in the crust[a]	Age (Ma)[a]	Mn/Fe[a]	Cu/Mn	Zn/Mn	Cu/Zn	Co/Mn	$\delta^{65/63}Cu_{NIST676}$	2sd[b]	$\delta^{66/64}Zn_{NIST3168a}$	2sd[b]	$\delta^{66/64}Zn_{JMC\text{-}Lyon}$
ZEP2-DR05-04 Fe-Mn crust													
ZEP2-DR05-04-L1	South Pacific	0.5	1.1	1.91	0.0022	0.0023	0.97	0.073	0.52	0.03	2.03	0.03	1.09
ZEP2-DR05-04-L2	South Pacific	1	1.7	1.66	0.0030	0.0025	1.22	0.066	0.51	0.03	2.04	0.03	1.10
ZEP2-DR05-04-L3	South Pacific	2.5	3.3	1.79	0.0036	0.0027	1.35	0.054	0.49	0.03	2.01	0.03	1.07
ZEP2-DR05-04-L4	South Pacific	3.5	3.9	1.52	0.0040	0.0030	1.33	0.050	0.51	0.03	2.00	0.03	1.06
ZEP2-DR05-04-L5	South Pacific	4.5	4.1	1.12	0.0044	0.0031	1.43	0.041	0.43	0.03	1.88	0.03	0.94
ZEP2-DR05-04-L6	South Pacific	6.5	4.6	1.05	0.0051	0.0031	1.62	0.045	0.34	0.03	1.83	0.03	0.89
ZEP2-DR05-04-L7	South Pacific	8.5	5.9	1.07	0.0053	0.0032	1.63	0.046	0.32	0.03	-	-	-
ZEP2-DR05-04-L8	South Pacific	10	6.5	1.04	0.0059	0.0035	1.69	0.049	0.27	0.03	1.74	0.03	0.80
ZEP2-DR05-04-L9	South Pacific	11.5	7.1	1.08	0.0058	0.0034	1.72	0.050	0.27	0.03	1.75	0.03	0.81
ZEP2-DR05-04-L10	South Pacific	12.5	7.7	1.03	0.0054	0.0032	1.69	0.055	0.32	0.03	1.76	0.03	0.82
ZEP2-DR05-04-L11	South Pacific	13.5	8.0	0.99	0.0058	0.0032	1.83	0.052	0.23	0.03	1.73	0.03	0.79
ZEP2-DR05-04-L12	South Pacific	15.5	8.6	1.02	0.0068	0.0036	1.87	0.052	0.24	0.03	1.74	0.03	0.80
ZEP2-DR05-04-L13	South Pacific	16.5	8.9	0.95	0.0063	0.0034	1.88	0.050	0.21	0.03	1.68	0.03	0.74
ZEP2-DR05-04-L14	South Pacific	17.5	9.6	1.14	0.0073	0.0041	1.79	0.049	0.21	0.03	1.76	0.03	0.82
ZEP2-DR05-04-L15	South Pacific	19	9.9	1.08	0.0074	0.0045	1.65	0.042	0.21	0.03	1.76	0.03	0.82
ZEP2-DR05-04-L16	South Pacific	20	10.4	1.27	0.0080	0.0047	1.71	0.051	0.19	0.03	1.76	0.03	0.82
ZEP2-DR05-04-L17	South Pacific	22	10.9	1.31	0.0101	0.0061	1.66	0.050	0.16	0.03	1.76	0.03	0.82
ZEP2-DR06-03 Fe-Mn crust													
ZEP2-DR06-03-L1	South Pacific	0.5	0.93	1.45	0.0026	0.0022	1.15	0.076	0.51	0.03	2.00	0.03	1.06
ZEP2-DR06-03-L2	South Pacific	2.5	2.14	1.27	0.0036	0.0025	1.48	0.063	0.44	0.03	1.99	0.03	1.05
ZEP2-DR06-03-L3	South Pacific	4	3.05	1.25	0.0039	0.0025	1.52	0.058	0.50	0.03	2.02	0.03	1.08
ZEP2-DR06-03-L4	South Pacific	5.5	3.96	1.14	0.0041	0.0027	1.55	0.057	0.46	0.03	2.02	0.03	1.08
ZEP2-DR06-03-L5	South Pacific	7.5	5.17	0.77	0.0054	0.0042	1.28	0.051	0.47	0.03	-	-	-
ZEP2-DR06-03-L6	South Pacific	9.5	5.54	1.17	0.0049	0.0027	1.84	0.051	0.48	0.03	1.90	0.03	0.96
ZEP2-DR06-03-L7	South Pacific	11	5.81	1.10	0.0056	0.0028	2.01	0.042	0.40	0.03	1.81	0.03	0.87
ZEP2-DR06-03-L8	South Pacific	12.5	5.88	1.02	0.0060	0.0029	2.06	0.047	0.34	0.03	1.73	0.03	0.79
ZEP2-DR06-03-L9	South Pacific	14	5.95	0.98	0.0067	0.0031	2.16	0.051	0.25	0.03	1.71	0.03	0.77
ZEP2-DR06-03-L10	South Pacific	16	6.05	0.94	0.0071	0.0033	2.14	0.051	0.27	0.03	1.63	0.03	0.69
ZEP2-DR06-03-L11	South Pacific	17.5	6.12	0.92	0.0075	0.0033	2.28	0.053	-	-	1.62	0.03	0.68
ZEP2-DR06-03-L12	South Pacific	19	6.29	0.99	0.0072	0.0032	2.26	0.051	0.21	0.03	1.63	0.03	0.69
ZEP2-DR06-03-L13	South Pacific	21	6.51	0.91	0.0076	0.0033	2.29	0.055	0.22	0.03	1.61	0.03	0.67
ZEP2-DR06-03-L14	South Pacific	23.5	6.91	0.98	0.0078	0.0034	2.33	0.052	0.18	0.03	1.61	0.03	0.67
J2-480 Fe-Mn crust													
J2-480-R1	North Pacific	0.2	7.13	1.18	0.0061	0.0053	1.14	0.025	0.73	0.06	2.10	0.04	1.16
J2-480-R2	North Pacific	2.5	7.40	1.44	0.0075	0.0041	1.81	0.023	0.54	0.06	2.19	0.04	1.25
J2-480-R3	North Pacific	5	7.69	1.40	0.0080	0.0046	1.74	0.023	0.59	0.06	2.10	0.04	1.16
J2-480-R4	North Pacific	7	7.93	1.55	0.0081	0.0041	1.96	0.029	0.66	0.06	2.13	0.04	1.19
J2-480-R5	North Pacific	9	8.16	2.22	0.0081	0.0033	2.41	0.024	0.65	0.06	2.19	0.04	1.25
J2-480-R6	North Pacific	11	8.39	1.72	0.0071	0.0035	2.04	0.023	0.67	0.06	2.18	0.04	1.24
J2-480-R7	North Pacific	12.5	8.57	1.69	0.0073	0.0039	1.88	0.020	0.64	0.06	2.14	0.04	1.20
J2-480-R8	North Pacific	14	8.74	1.75	0.0076	0.0038	1.97	0.017	0.66	0.06	2.13	0.04	1.19
J2-480-R9	North Pacific	15	9.40	1.28	0.0086	0.0042	2.03	0.018	0.63	0.06	2.15	0.04	1.21
J2-480-R10	North Pacific	16.5	10.39	0.69	0.0111	0.0054	2.05	0.014	0.56	0.06	1.97	0.04	1.03
J2-480-R12	North Pacific	19	12.04	0.68	0.0126	0.0048	2.66	0.015	0.57	0.06	1.91	0.04	0.97
J2-480-R14 Fe-Mn crust													
J2-480-R14-L11	North Pacific	0.2	3.69	1.32	0.0046	0.0055	0.84	0.030	0.65	0.06	2.19	0.04	1.25
J2-480-R14-L10	North Pacific	3	5.47	1.21	0.0055	0.0073	0.75	0.029	0.63	0.06	2.16	0.04	1.22
J2-480-R14-L9	North Pacific	5	6.75	1.35	0.0057	0.0063	0.91	0.032	0.66	0.06	2.06	0.04	1.12
J2-480-R14-L8	North Pacific	7	7.81	1.67	0.0053	0.0036	1.45	0.031	0.65	0.06	2.14	0.04	1.20
J2-480-R14-L7	North Pacific	9	8.87	1.71	0.0059	0.0036	1.65	0.037	0.72	0.06	2.18	0.04	1.24
J2-480-R14-L6	North Pacific	10	9.40	1.79	0.0060	0.0042	1.41	0.036	0.67	0.06	2.18	0.04	1.24
J2-480-R14-L5	North Pacific	12	10.46	1.30	0.0073	0.0043	1.70	0.038	0.67	0.06	2.12	0.04	1.18
J2-480-R14-L4	North Pacific	14	11.51	1.64	0.0065	0.0046	1.40	0.034	0.69	0.06	2.20	0.04	1.26
J2-480-R14-L3	North Pacific	16	12.37	1.57	0.0064	0.0035	1.84	0.024	0.63	0.06	2.09	0.04	1.15
J2-480-R14-L2	North Pacific	18	13.23	1.26	0.0082	0.0042	1.95	0.026	0.60	0.06	2.05	0.04	1.11
J2-480-R14-L1	North Pacific	20	16.98	1.25	0.0085	0.0042	2.02	0.025	0.56	0.06	2.03	0.04	1.09
Bulk Fe-Mn crusts													
CAP BREST 03-03	Atlantic (Ascension FZ)	-	-	0.53	0.0061	0.0036	1.68	0.023	0.22	0.02	1.66	0.05	0.72
DR01-003 4-B-5	Atlantic (VEMA FZ)	-	-	0.59	0.0080	0.0039	2.06	0.026	0.31	0.01	1.52	0.05	0.58
DR-01-005 16-A-12	Atlantic (VEMA FZ)	-	-	0.66	0.0061	0.0036	1.68	0.038	0.23	0.01	1.56	0.02	0.62
DR01-005 16-A-6	Atlantic (VEMA FZ)	-	-	0.61	0.0071	0.0040	1.79	0.022	0.23	0.00	1.56	0.05	0.62
DR01-005 16-B-11	Atlantic (VEMA FZ)	-	-	0.66	0.0051	0.0036	1.40	0.028	0.25	0.02	1.62	0.05	0.68
DR01-005 16-B-12	Atlantic (VEMA FZ)	-	-	0.72	0.0047	0.0036	1.30	0.036	0.52	0.01	1.69	0.05	0.75
DR01-005 6-C-13	Atlantic (VEMA FZ)	-	-	0.79	0.0052	0.0037	1.39	0.039	0.16	0.02	1.73	0.05	0.79
DR03-003 17-C-4	Atlantic (VEMA FZ)	-	-	0.60	0.0048	0.0042	1.15	0.025	0.54	0.02	1.65	0.05	0.71
DR03-025 15#5	Atlantic (VEMA FZ)	-	-	0.61	0.0055	0.0040	1.37	0.022	0.26	0.03	1.68	0.05	0.74
DR03-025 15-D-10	Atlantic (VEMA FZ)	-	-	0.56	0.0075	0.0044	1.68	0.025	0.21	0.03	1.60	0.05	0.66
DR12-24 32-A-6	Atlantic (Gloria FZ)	-	-	0.67	0.0068	0.0044	1.53	0.021	0.21	0.02	1.77	0.05	0.83
DR12-24 32-B-2	Atlantic (Gloria FZ)	-	-	0.74	0.0056	0.0038	1.47	0.030	0.21	0.02	1.76	0.05	0.82
DR12-24 32-B-3-1	Atlantic (Gloria FZ)	-	-	0.67	0.0067	0.0043	1.55	0.028	0.30	0.03	1.75	0.05	0.81
DR12-24 32-B-3-2	Atlantic (Gloria FZ)	-	-	0.69	0.0062	0.0043	1.44	0.027	0.15	0.02	1.73	0.05	0.79
DR24-09 34-A-2-1	Atlantic (Azores TJ)	-	-	2.58	0.0023	0.0023	0.98	0.047	0.25	0.02	1.95	0.05	1.01
DR-24-09 34-A-2-2	Atlantic (Azores TJ)	-	-	2.56	0.0022	0.0023	0.97	0.046	0.19	0.01	1.96	0.05	1.02
DR24-09 34-C-2-1	Atlantic (Azores TJ)	-	-	2.43	0.0027	0.0023	1.17	0.053	0.53	0.00	1.94	0.05	1.00
DR24-09 34-C-2-1	Atlantic (Azores TJ)	-	-	2.48	0.0030	0.0024	1.26	0.054	0.17	0.01	1.94	0.05	1.00
J2-480-R11	North Pacific (Hawaii)	-	-	1.12	0.0069	0.0035	1.98	0.015	0.28	0.04	1.86	0.05	0.92
J2-480-R13A	North Pacific (Hawaii)	-	-	1.24	0.0080	0.0027	2.92	0.022	0.48	0.01	1.97	0.05	1.03
Nod-A-1[c]	Atlantic	-	-	-	-	-	-	-	0.29	0.09	1.89	0.07	0.95
Nod-P-1[c]	Pacific	-	-	-	-	-	-	-	0.34	0.05	1.74	0.12	0.80

[a]Age (Ma) were calculated using cosmogenic ^{10}Be isotope, except sample ZEP2-DR05-04 dated with the Co-method. The age data and elemental data are already published in Gueguen et al. (2016).
[b]2sd stands for two-standard deviation calculated on replicate measurements of NIST976 for Cu isotopes and NIST3168a for Zn isotopes, except for Nod-A-1 and Nod-P-1 which corresponds to digested and column procedure duplicates and replicate measurements on the mass spectrometer.
[c]Average of digested and column procedure duplicates of Nod-A-1 and Nod-P-1.